Cenozoic tectonic evolution of the White Mountains, California and Nevada

Daniel F. Stockli†
Department of Geology, University of Kansas, Lawrence, Kansas 66045, USA, and *Department of Geological and Environmental Sciences, Stanford University, Stanford, California 94305-2115, USA*

Trevor A. Dumitru
Michael O. McWilliams
Department of Geological and Environmental Sciences, Stanford University, Stanford, California 94305-2115, USA

Kenneth A. Farley
Division of Geological and Planetary Sciences, MS 170-25, California Institute of Technology, Pasadena, California 91125, USA

ABSTRACT

The White Mountains represent the westernmost range of the central northern Basin and Range province. They are situated to the east of the unextended Sierra Nevada and represent a crustal block that is bounded along its western flank by the high-angle White Mountains fault zone. The fault zone accommodates up to ~8 km of total dip-slip displacement. Investigation of the structural and thermal history of the White Mountains indicates a two-stage Cenozoic tectonic evolution. Preextensional Miocene volcanic rocks preserved along the eastern side of the range unconformably overlie Mesozoic granitic basement and currently dip up to 25° to the east, recording the total Cenozoic tilt of the crustal block. Apatite fission-track and (U-Th/He) thermochronological data indicate that the White Mountains underwent rapid exhumation and eastward tilting in the middle Miocene, starting at ca. 12 Ma. Geologic mapping (1:10,000), fault kinematic analysis, and dating of younger volcanic sequences show that following middle Miocene east-west extension, the White Mountains have been dominated by right-lateral transtensional deformation related to the Walker Lane belt. The eruption of late Miocene and Pliocene volcanic sequences in the eastern White Mountains postdates the majority of the uplift of the range, as evidenced by infilling of paleodrainages and the presence of east-directed flow fabrics. Fault kinematic indicators from the White Mountains fault zone are characterized by apparent overprinting of dip-slip fault-motion indicators by right-lateral slickenfibers and fault striations, demonstrating that the range-bounding fault system along the western side of the White Mountains was reactivated as a dextral strike-slip fault system. At the northern and southern ends of the range, Pliocene right-lateral transtension along this northwest–southeast-trending fault systems resulted in the formation of northeast-trending pull-apart basins that truncate the mountain range and transfer strike-slip displacement eastward from the Owens Valley fault zone to the Fish Lake Valley fault zone. The inception of strike-slip faulting in Fish Lake Valley occurred at ca. 6 Ma as constrained by late Miocene volcanic units. Right-lateral faulting on the western side of the White Mountains occurred at ca. 3 Ma and is distinctly younger than the faulting in the Fish Lake Valley area, indicating a westward migration of transcurrent deformation through time.

Keywords: White Mountains, Basin and Range, Walker Lane belt, tectonics, thermochronology.

INTRODUCTION

Many details of the temporal and spatial distribution of extensional and transtensional faulting in the northern Basin and Range province are only poorly constrained, despite decades of structural and geochronological studies. In particular, the relationships between extensional faulting in the western Basin and Range province and the transcurrent structures of the Walker Lane belt remain controversial (Fig. 1). The marked physiographic and tectonic differences between the central Basin and Range and the Walker Lane belt have long been recognized (e.g., Locke et al., 1940). The central part of the northern Basin and Range province, with its evenly spaced, north-trending mountain ranges, contrasts with the Walker Lane belt in the western part of the province that is characterized by a complicated array of predominantly northwest-trending, right-lateral strike-slip and transtensional faults (Hardyman and Oldow, 1991; Stewart, 1992a, 1992b; Oldow, 1992).

The White Mountains of eastern California and western Nevada (Fig. 1) represent the westernmost range-forming crustal fault block of the central part of the northern Basin and Range province east of the Sierra Nevada, although they are currently situated within the broad zone of right-lateral faulting associated with the Walker Lane belt (Figs. 1 and 2). The White Mountains exhibit evidence for both extensional and right-lateral strike-slip faulting, based on previous work by DePolo (1989) and relationships presented in this study. The physiography and high elevation of the White Mountains can primarily be attributed to the fact that the range is a north-trending, east-tilted crustal block bounded on the west by a normal fault with as much as ~8 km of dis-

†E-mail: stockli@ku.edu.

GSA Bulletin; July 2003; v. 115; no. 7; p. 788–816; 19 figures; 4 tables Data Repository item 2003094.

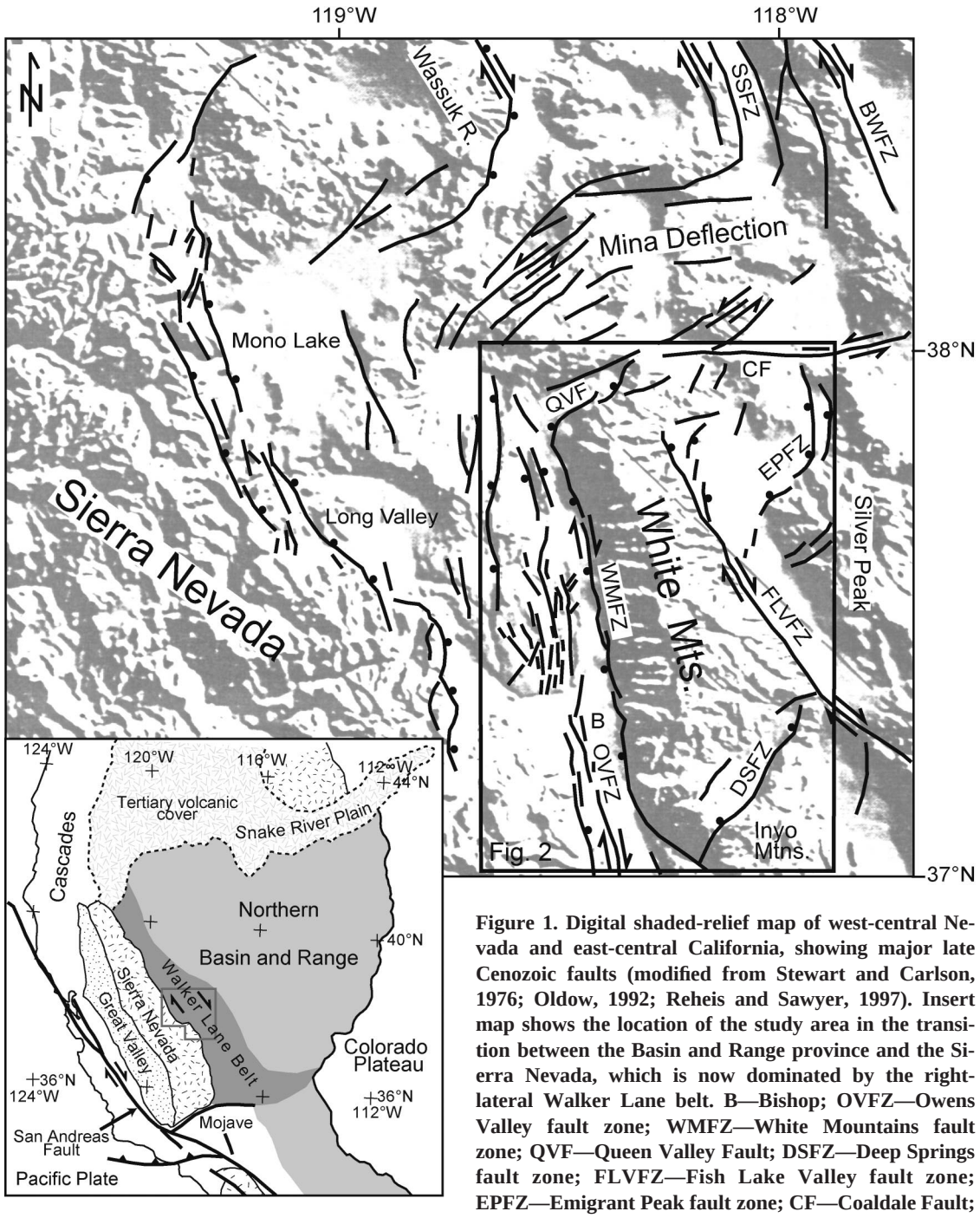

Figure 1. Digital shaded-relief map of west-central Nevada and east-central California, showing major late Cenozoic faults (modified from Stewart and Carlson, 1976; Oldow, 1992; Reheis and Sawyer, 1997). Insert map shows the location of the study area in the transition between the Basin and Range province and the Sierra Nevada, which is now dominated by the right-lateral Walker Lane belt. B—Bishop; OVFZ—Owens Valley fault zone; WMFZ—White Mountains fault zone; QVF—Queen Valley Fault; DSFZ—Deep Springs fault zone; FLVFZ—Fish Lake Valley fault zone; EPFZ—Emigrant Peak fault zone; CF—Coaldale Fault; SSFZ—Soda Springs fault zone; and BWFZ—Bettles Well fault zone. Normal faults have balls on downthrown side.

placement, primarily accumulated during the Miocene (Fig. 2). The younger history of the range, however, is dominated by transcurrent faulting. At present, the range is bounded on both its eastern and western flanks by seismically active, right-lateral strike-slip faults. The Fish Lake Valley and the Owens Valley strike-slip fault zones, like most northwest-trending strike-slip faults in the Walker Lane belt (Fig. 1), are characterized by late Cenozoic right-lateral displacement with a minor dip-slip component (e.g., Reheis and Dixon, 1996; Reheis and Sawyer, 1997). Local and regional geodetic studies have demonstrated that as a group, these northwest-trending faults accommodate right-lateral shearing within the western part of the northern Basin and Range province (e.g., Savage, 1983; Dixon et al., 1995, 2000; Miller et al., 2001). This study integrates structural, geochronological, and thermochronological techniques to determine the Cenozoic tectonic evolution of the White Mountains area and more specifically to resolve controversy re-

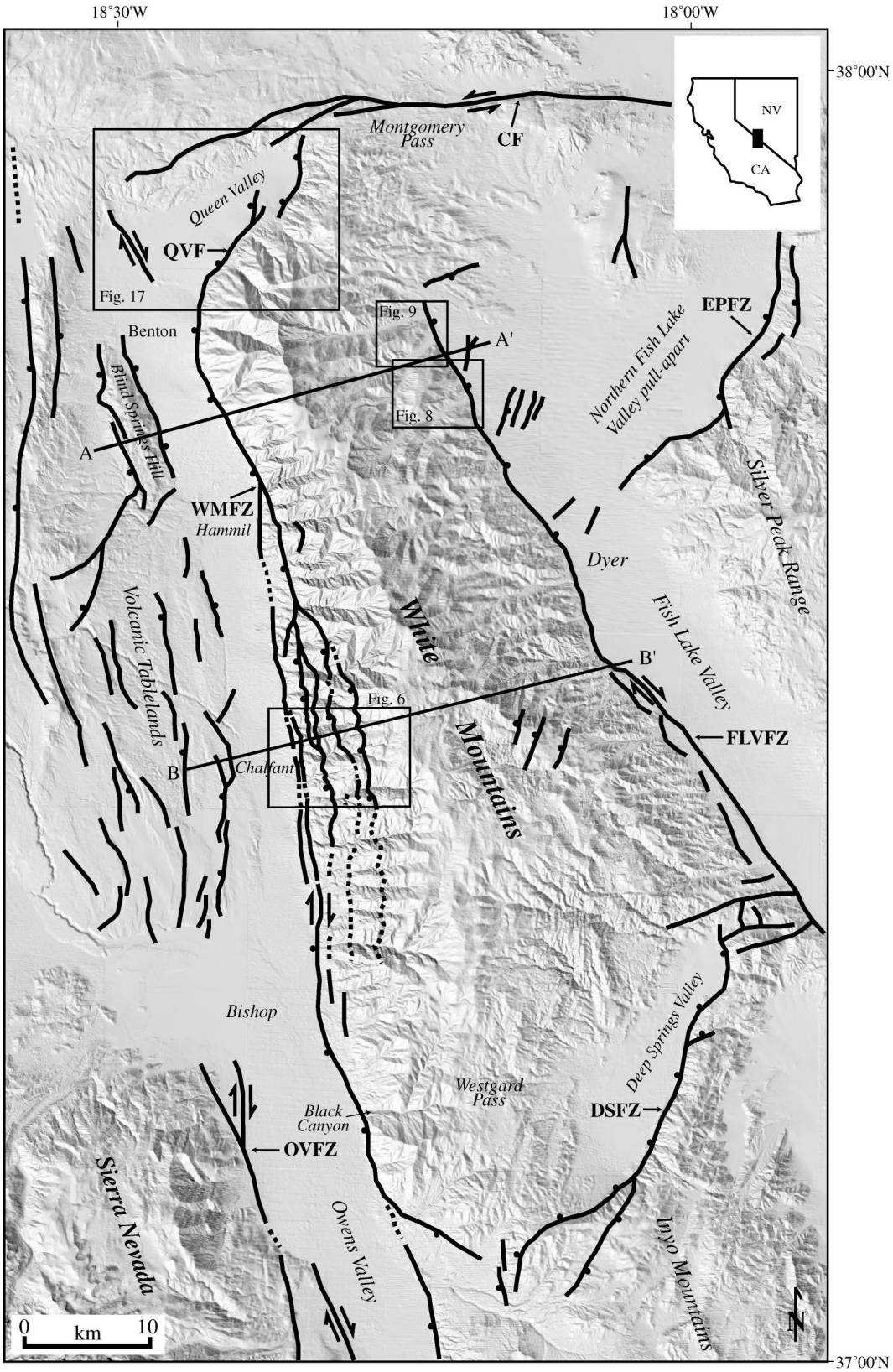

Figure 2. Digital shaded-relief map of White Mountains, east-central California and west-central Nevada, showing late Cenozoic faults and locations of cross sections (A–A′ and B–B′, Fig. 4). Faults after Stewart and Carlson (1976), DePolo (1989), Reheis and Sawyer (1997), and Lee et al. (2001). Shaded-relief map generated from U.S. Geological Survey digital elevation model (DEM) data. For fault abbreviations, see Figure 1. Boxes show locations of Figures 6, 8, 9, and 17.

garding the temporal and spatial relationship and geometric interplay between extensional and transcurrent tectonic elements in the White Mountains area.

GEOLOGIC SETTING OF THE WHITE MOUNTAINS

The White Mountains share a common Paleozoic and Mesozoic tectonic and magmatic history with the Sierra Nevada, of which they were a part, prior to Basin and Range extension. Pre-Cenozoic rocks in the southern White Mountains, south of Mount Barcroft (Fig. 3), consist of sedimentary rocks of late Precambrian and early Paleozoic age as well as several Mesozoic granitic intrusions (Crowder and Ross, 1972; Ernst, 1987). The area north of Mount Barcroft is mainly underlain by Jurassic and Cretaceous granitic plutons and Mesozoic metavolcanic and metasedimentary rocks (Krauskopf, 1968; Crowder et al., 1973; Hanson, 1986, 1997; Hanson et al., 1987; McKee and Conrad, 1996). The northern White Mountains are dominated by several large plutonic complexes, including the Jurassic (ca. 160 Ma) Barcroft Granodiorite, the Early to middle Cretaceous (ca. 130 Ma) composite Pellisier Flat pluton and McAfee pluton, and the Late Cretaceous (ca. 73 Ma) leucocratic Boundary Peak Granite (e.g., Crowder et al., 1973; McKee and Conrad, 1996; Hanson, 1997) (Fig. 3).

Most of the metamorphic history and the development of penetrative deformational fabrics in the White Mountains are attributed to tectonism accompanying arc magmatism in the Late Jurassic to Late Cretaceous occurring in concert with arc magmatism (Dunne, 1986; Stevens et al., 1997). Cretaceous mylonitic fabrics associated with the White Mountains shear zone (to the east of the White Mountains fault zone; Fig. 3) are widespread along the western flank of the northern White Mountains (Dunne et al., 1978; Hanson, 1987). These mylonites are best developed in the Pellisier Flat pluton, where abundant S-C fabrics indicate a top-to-the-east sense of shear (Hanson, 1987). The mylonites are intruded by the Late Cretaceous Boundary Peak Granite and associated aplitic dikes, indicating that motion along the White Mountains shear zone had ceased by that time (Fig. 3) (Hanson, 1987; Stockli, 1999). The Mesozoic White Mountains shear zone strongly influenced the geometry of the Cenozoic White Mountains fault zone along the western flank of the White Mountains, and the anisotropy of the Cretaceous mylonites controls the location of the Cenozoic range-bounding normal fault at least in the northern part of the range (Fig. 4;

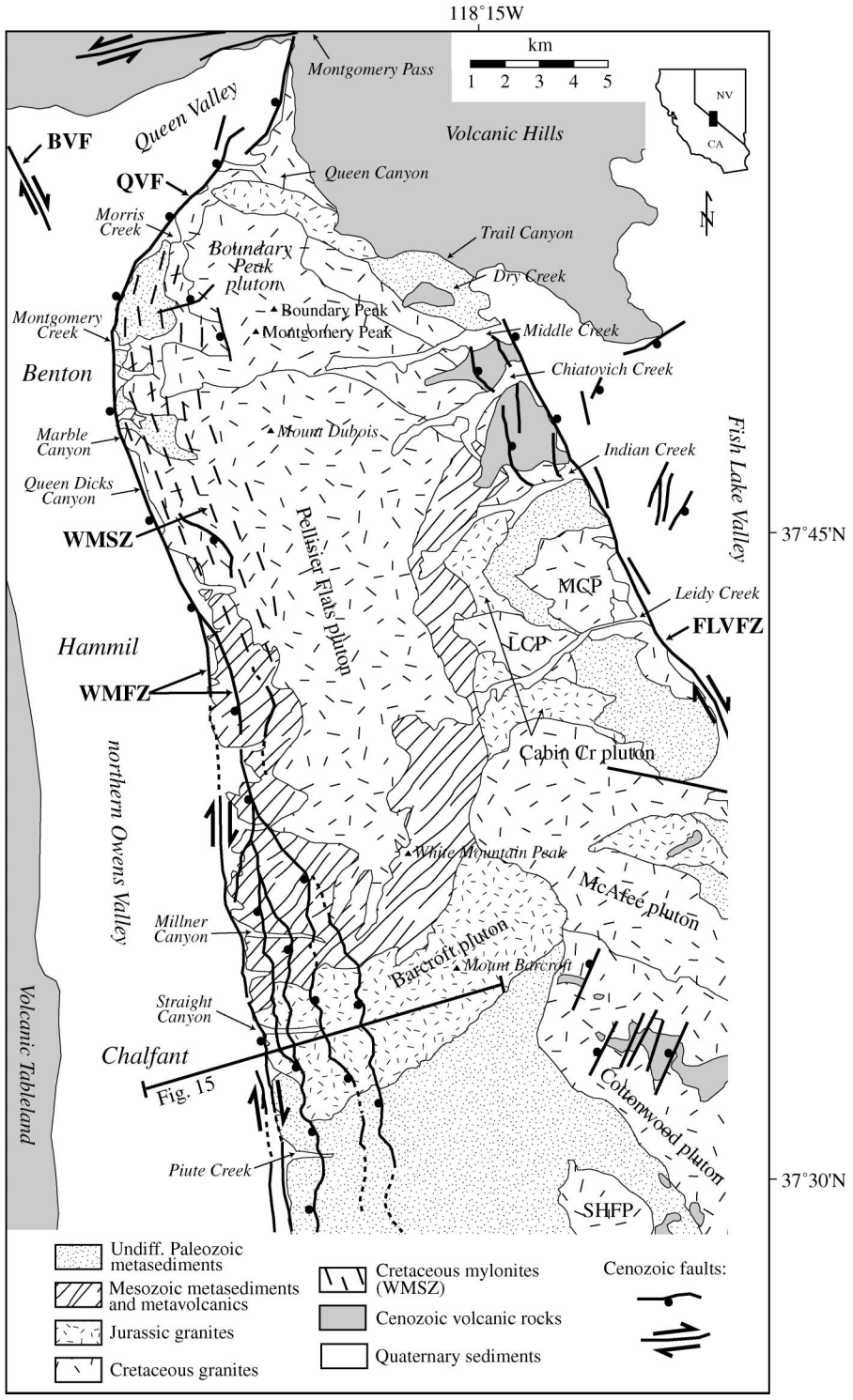

Figure 3. Simplified geologic map of the northern and central White Mountains, showing the distribution of Precambrian to Mesozoic metasedimentary and igneous rocks, as well as Cenozoic faults and volcanic rocks (modified after McKee et al., 1982). Granitic plutons: SHFP—Sage Hen Flat pluton; MCP—Marble Creek pluton; LCP—Leidy Creek pluton. Faults and shear zones: BVF—Benton Valley Fault; FLVFZ—Fish Lake Valley fault zone; QVF—Queen Valley Fault; WMFZ—White Mountains fault zone; WMSZ—White Mountains shear zone. Location of cross section in Figure 15 is shown.

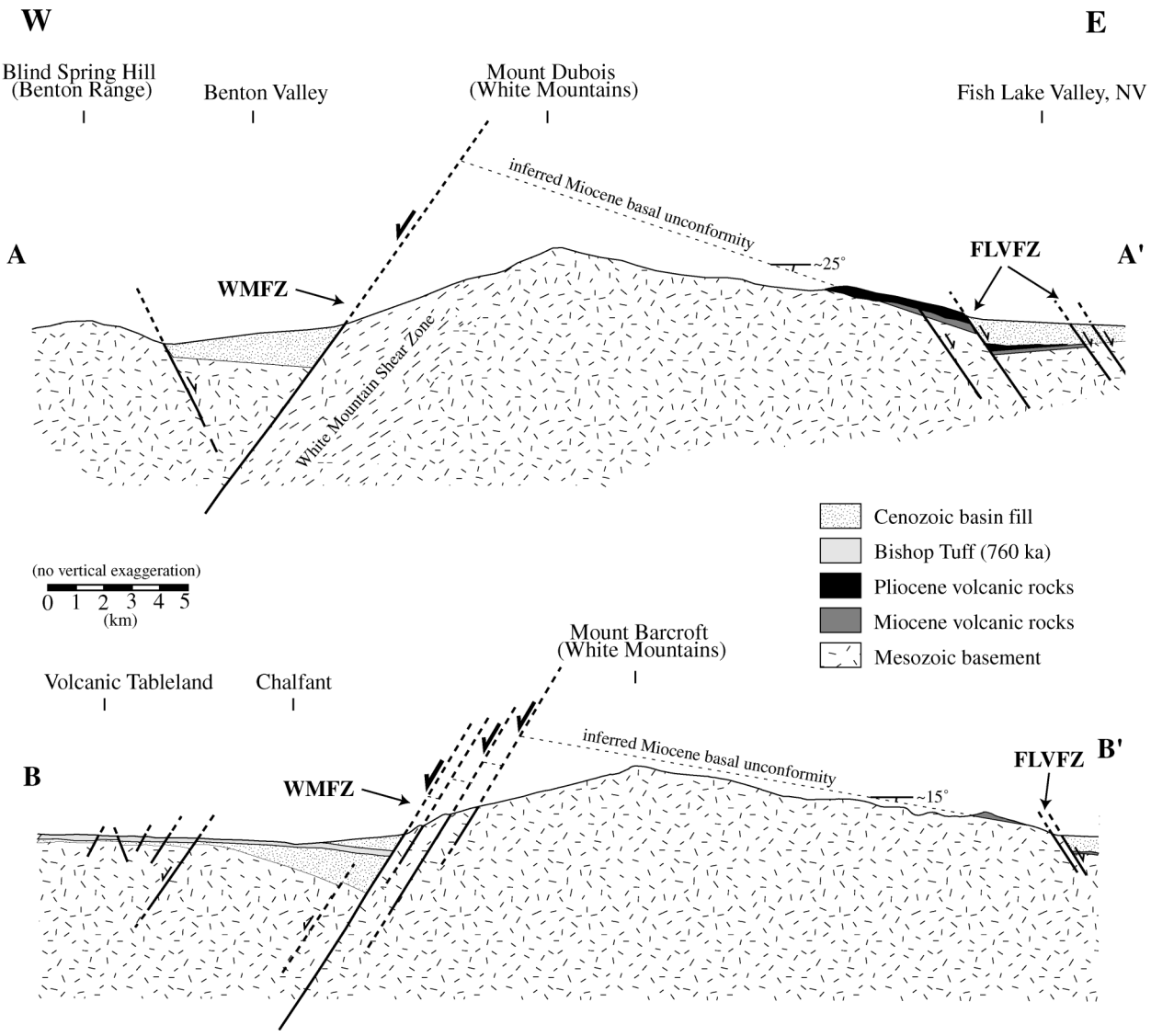

Figure 4. Simplified east-west cross sections of the northern (A–A′) and central (B–B′) White Mountains. The White Mountains fault block represents an east-tilted crustal block bounded along the western flank by the White Mountains fault zone (WMFZ). Minor faults along the eastern side of the range are related to faulting along the Fish Lake Valley fault zone (FLVFZ). Structural reconstruction is based on the tilted middle Miocene basal unconformity on the eastern side of the White Mountains (see text for details) and fault kinematic data of the White Mountains fault zone (Fig. 5). Locations of cross sections A–A′ and B–B′ are shown on Figure 2.

DePolo, 1989). The White Mountains fault zone extends for ~80 km from Montgomery Pass in the north to Deep Springs Valley in the south and forms a major escarpment with up to 3 km topographic relief (Figs. 2 and 4). Geophysical studies in the adjacent northern Owens Valley, which includes Chalfant, Hammil, and Benton Valleys (Fig. 4), suggest that the basin underlying northern Owens Valley has a half-graben geometry with up to ~2 km of sedimentary fill (Pakiser et al., 1964; Russell, 1977). Gravity data also indicate that the half graben is segmented into subbasins by northwest-trending, fault-bounded basement highs (Pakiser et al., 1964).

Figure 5. Lower-hemisphere equal-area stereographic plots of fault kinematic data from the White Mountains fault zone (WMFZ). Plots show orientation of striations with sense of displacement of hanging wall (left), fault-plane orientations as great circles (middle), and contoured slip directions (contour interval 3×) (right). (A) Faults within the range in the central White Mountains are characterized by dip-slip motion. (B) Faults along the range front exhibit mostly subhorizontal slickenfibers and striations indicative of right-lateral strike-slip faulting. (C and D) Fault planes in the northern White Mountains exhibit two sets of fault kinematic indicators; the apparently younger set of slickenfibers signify right-lateral oblique-slip fault motion. (E) Fault kinematic data from the Queen Valley Fault indicate down-to-the-northwest dip-slip motion along northeast-striking faults. Diagrams prepared with Stereoplot program by N. Mancktelow.


Slickenfibers and striations
Fault plane data
Contoured fault slip directions
(A)
WMFZ within range
(Barcroft)
mean fault plane
261/51 (n=36)
dip-slip
striations
fault planes
(n=36)
mean fault plane
261/51 (n=36)
249/51
32 Data
(B)
WMFZ at range front
(Barcroft)
oblique-slip
striations
dip-slip
striations
mean fault plane
255/50 (n=26)
fault planes
(n=26)
332/18
253/50
mean fault plane
255-50 (n=26)
26 Data
(C)
WMFZ at Queen
Dicks Creek
oblique-slip
striations
dip-slip
striations
mean fault plane
246-55 (n=29)
fault planes
(n=29)
318/24
226/57
mean fault plane
246-55 (n=29)
29 Data
(D)
WMFZ at
Marble Canyon
oblique-slip
striations
antithetic
faults
dip-slip
striations
mean fault plane
257/55 (n=39)
antithetic
faults
fault planes
(n=39)
341/18
antithetic
faults
264/58
mean fault plane
257/55 (n=39)
39 Data
(E)
Queen Valley
dip-slip
striations
mean fault plane
329/552 (n=56)
fault planes
(n=56)
335/52
329/552 (n=56)
47 Data

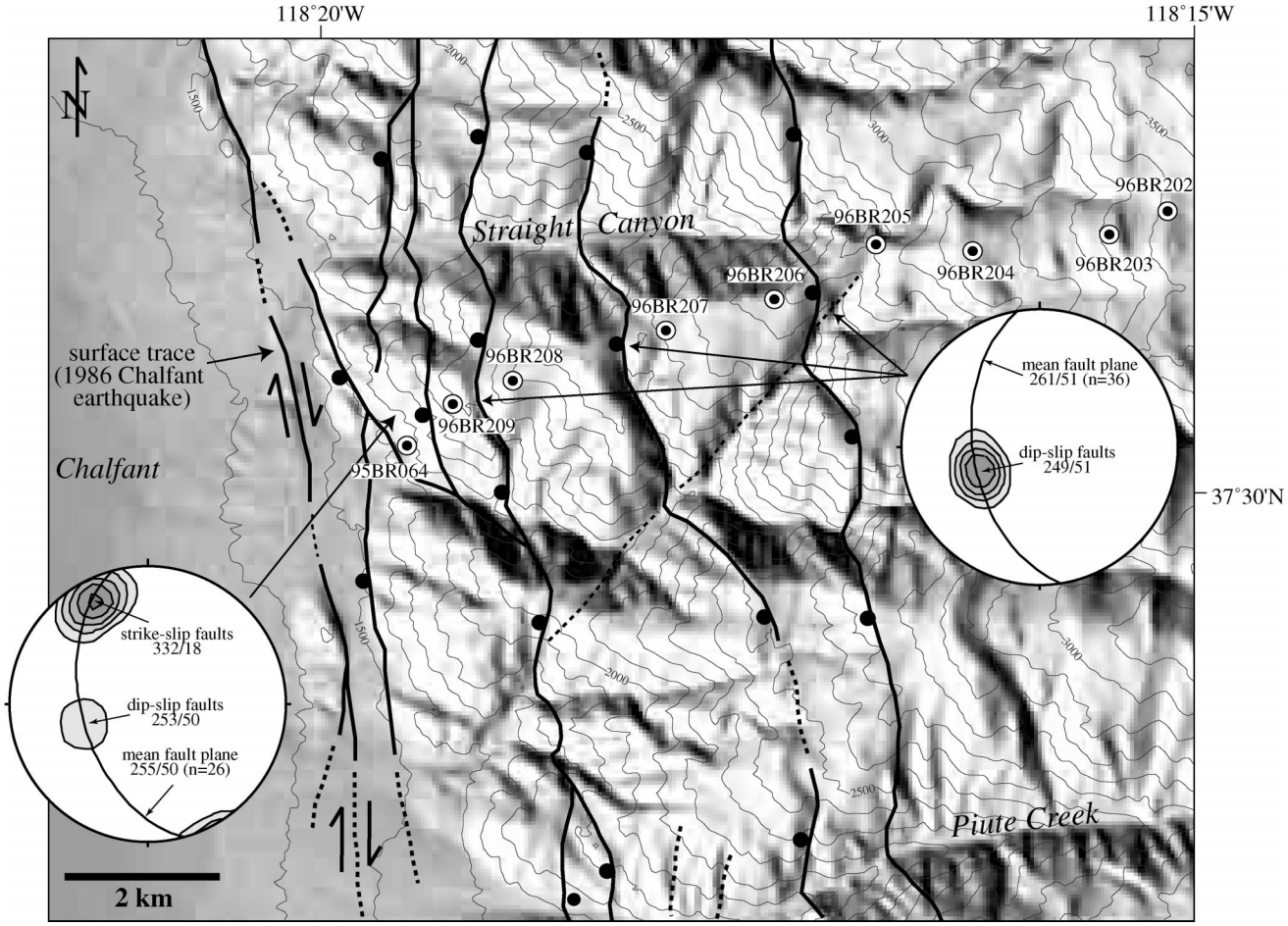

Figure 6. Digital shaded-relief map of the western flank of the central White Mountains east of Chalfant, showing the major Cenozoic west-dipping normal faults of the White Mountains fault zone that accommodate progressive down-to-the-west normal displacement (ball on down-dropped side). Contoured summary stereonets of fault kinematic data illustrate the predominant dip-slip displacement along the faults of the White Mountains fault zone and subsequent reactivation of the range-bounding fault as a right-lateral strike-slip fault, as indicated by a second set of subhorizontal slickenfibers and striations. Also shown is the surface trace of the 1986 Chalfant earthquake ruptures that illustrate the present-day right-lateral sense of fault motion along the range front. Sample numbers and locations (Table 4) correspond to fission-track and (U-Th)/He thermochronological sample transect shown in Figure 15. Contour interval is 100 m.

STRUCTURAL GEOLOGY AND FAULT KINEMATICS

The geology of the White Mountains is well mapped at 1:62,500 (for compilation, see McKee et al., 1982), and much of the analysis of the structure of the range discussed herein builds on these previous field studies. In the work described here, the main fault strands of the White Mountains fault zone, as well as subsidiary faults along the western flank of the White Mountains and the Queen Valley Fault, were mapped and studied in detail to better understand their movement history. Information on the slip history of these fault systems was collected from three key areas: the central White Mountains east of Chalfant, the northern White Mountains between Hammil and Benton, and Queen Valley at the northern end of the range (Figs. 2, 5, and 6).

Chalfant Area

In the Chalfant area, the White Mountains fault zone includes several parallel normal-fault strands that have been mapped to the east of the main range-bounding fault within the range (Fig. 6). East of Chalfant within the Jurassic Barcroft pluton (Figs. 3 and 6), the fault zone encompasses four east-dipping normal faults, including the main range-front fault, that together accommodate a total dip-slip displacement of ~5–6 km in a step-like fashion (Fig. 4). The three faults mapped within the range are relatively discrete fault zones that are characterized by polished, iron oxide–stained fault planes with a mean orientation of 261°/51°. The surrounding granitic rocks show little evidence for subsidiary faulting or hydrothermal alteration. Slickenfibers and striations are well developed and indicative of down-to-the-west normal displacement (Fig. 5A). Figure 5A illustrates that the fault motion, as indicated by the striations (249°/51°), is almost purely dip slip with respect to the average fault-plane orientation (261°/51°). The amount of dip-slip displacement along these three faults is difficult to assess owing to the lack of easily recognized offset geologic markers. However, on the basis of thermo-

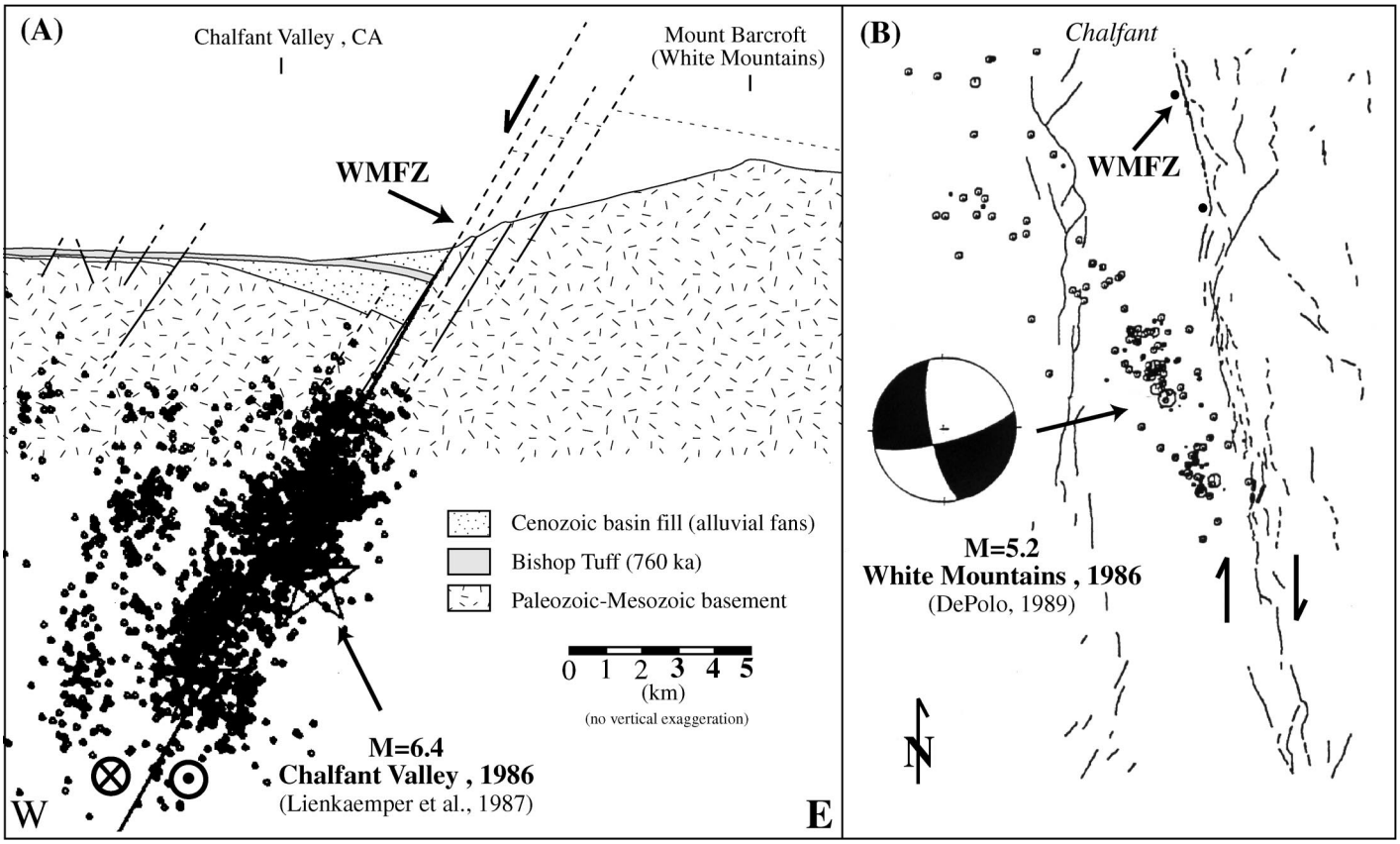

Figure 7. Modern seismicity along the western side of the White Mountains demonstrates the reactivation of the White Mountains fault zone (WMFZ) as a right-lateral strike-slip fault system. (A) Cross section of the central White Mountains (same as Fig. 4B) shows the preextensional Miocene basal unconformity illustrating the east-tilted fault-block geometry of the central White Mountains as a result of middle Miocene east-west extension. The magnitude 6.4 Chalfant Valley earthquake nucleated along a fault oblique to the White Mountains fault zone, but secondary coseismic motion appears to have occurred along the White Mountains fault zone and is characterized by right-lateral surface fractures (e.g., Lienkaemper et al., 1987; DePolo, 1989). (B) The White Mountains earthquake (M = 5.2), part of the Chalfant Valley earthquake swarm, occurred along a west-dipping fault plane that appears to represent the subsurface continuation of the White Mountains fault zone. The focal mechanism of the White Mountains earthquake indicates dextral fault slip along the fault zone, further corroborating the reactivation of the fault zone in a transcurrent fashion (modified after DePolo, 1989).

chronology data discussed later in this paper, these faults are each inferred to have down-to-the-west normal offsets of 1–1.5 km; therefore, these faults accommodate a total displacement of ~5 km across the White Mountains fault zone (Fig. 4B).

Along the range-front fault in the Chalfant area, the granitic rocks of the Barcroft pluton are intensely hydrothermally altered and mineralized and exhibit abundant subsidiary minor-displacement faults with stepped epidote and calcite slickenfibers, indicating right-lateral oblique displacement (Fig. 5B). Only rare occurrences of striations indicating dip-slip motion were observed on these fault planes.

Recent earthquakes and aftershock sequences provide insights into the modern kinematics of faulting along the western flank of the White Mountains (DePolo, 1989) (Fig. 7). Earthquake focal-mechanism and aftershock studies of the Ms = 6.6 Chalfant event (July 21, 1986) indicate that coseismic displacement was dominantly right-lateral strike-slip. DePolo (1989) suggested that the main shock along a concealed northwest-striking fault plane dynamically triggered right-lateral slip along the White Mountains fault zone. Coseismic surface ruptures have a length of ~15.5 km and are characterized by dextral oblique offsets with a maximum displacement of 5 cm (DePolo and Ramelli, 1987).

The Ms = 5.2 White Mountains earthquake (July 31, 1986) and aftershocks appear to have occurred along the White Mountains fault zone itself north of Chalfant (DePolo, 1989). The focal mechanism of the White Mountains earthquake indicates right-lateral motion. Furthermore, in cross-sectional view, the distribution of aftershocks outline a west-dipping fault plane, similar in orientation to the nodal plane of the main shock (Fig. 7) (DePolo, 1989). The up-dip projection of the seismic fault plane intersects the surface at the western range front of the White Mountains and appears to be the subsurface projection of the White Mountains fault zone.

Northern White Mountains Area

In the northern White Mountains, north of Hammil and south of Benton, the White Mountains fault zone consists of a single master fault along the range front with no evidence for significant subsidiary faulting within the range (Figs. 2, 3, and 4A). Footwall rocks are characterized by west-dipping mylonitic fabrics of the Cretaceous White Mountains shear zone, and these strongly anisotropic, planar fabrics may have helped to localize

slip along a single range-front fault. Fault kinematic data were collected from small-displacement faults that are subsidiary to the main range-bounding fault zone in the Queen Dicks Canyon and Marble Canyon areas along the western range front (Figs. 2, 3, 5C, and 5D). Two populations of slickenfibers and striations were observed on the same minor fault planes developed in strongly altered and epidotized/chloritized Pellisier Flat Granite (Figs. 5C, 5D). The average fault-plane orientation is 246°/55° in the Queen Dicks Canyon area and 257°/55° in the Marble Canyon area (Fig. 5C). Individual faults often exhibit faint dip-slip striations with superimposed calcite and epidote slickenfibers on the same fault planes. The older population indicates predominantly normal-sense fault motion, similar to faults in the interior of the central White Mountains (Fig. 5A). The younger, better-developed population of slickenfibers indicates right-lateral oblique fault motion, suggesting that normal displacement along the western flank of the White Mountains predates reactivation of the White Mountains fault zone as a right-lateral strike-slip fault.

Queen Valley Area

In the Queen Valley area, at the northern end of the White Mountains, the orientation of the White Mountains fault zone changes rather abruptly from approximately north-south to northeast-southwest (Fig. 3). Here this fault segment is termed the ''Queen Valley Fault.'' Fault kinematic data from the northeast-trending Queen Valley Fault indicate that fault motion is dominated by down-to-the-northwest dip-slip displacement (Fig. 5E). Northeast-trending small-displacement faults indicate almost pure dip-slip motion, whereas more due east–trending fault planes are in general characterized by an increased sinistral-slip component. Holocene fault scarps along the range front and in alluvial fans at the mouth of Queen Canyon also suggest down-to-the-northwest displacement, accommodating northwest-southeast extension (DePolo, 1989). The fault kinematics suggest an extension direction of ~335° (Fig. 5E).

Near Montgomery Pass (Fig. 2), the Queen Valley Fault appears to be truncated by or, more likely, to merge with the Coaldale Fault. The Coaldale Fault represents an east-trending left-lateral strike-slip fault that transfers displacement from the northern end of the Owens Valley fault zone to the southern end of the central Walker Lane belt in a regional-scale right step (Speed, 1979; Oldow, 1992) (Fig. 1). This kinematic interpretation of the Coaldale Fault is in good agreement with earthquake focal mechanisms that suggest predominantly left-lateral oblique-slip displacement along the east-trending faults in the Excelsior-Coaldale domain of the Mina deflection (Rogers et al., 1991; Oldow, 1992; Oldow et al., 1994) (Fig. 1).

Summary

The fault-slip data suggest that extensional faults bounding the White Mountains crustal block have been overprinted and reactivated by strike-slip faulting along the White Mountains range front. Analysis of active fault scarps and earthquake data along the central part of the western range front illustrates that the present-day sense of displacement along the White Mountains fault zone is predominately right-lateral strike-slip (Bryant, 1984; Cockerham and Corbett, 1987; DePolo and Ramelli, 1987; Lienkaemper et al., 1987; DePolo, 1989; DePolo et al., 1993). More precise constraints on the timing of this transition in fault kinematics have been explored in this study by using geochronological and thermochronological tools, as detailed subsequently.

TILTING CONSTRAINTS BASED ON CENOZOIC VOLCANIC ROCKS

Volcanic deposits in the White Mountains area (Fig. 3) consist of regionally extensive Oligocene to middle Miocene rhyolite and basalt, Miocene andesitic flows and tuffaceous sedimentary rocks, and voluminous late Miocene and Pliocene andesite and basaltic andesite flows (Crowder et al., 1972; Robinson and Stewart, 1984). Late Pliocene and Quaternary volcanism is characterized by widespread olivine basalt flows that unconformably overlie the older rocks. These Cenozoic volcanic deposits provide important constraints on the amount and timing of eastward tilting of the White Mountains, which is crucial for the interpretation of the thermochronology data. Detailed mapping (1:10,000) of the volcanic sequences along the eastern flank of the White Mountains between Indian Creek and Trail Canyon (Figs. 3, 8, 9) was complemented with $^{40}Ar/^{39}Ar$ age determinations. In summary, these data show (1) that the range underwent ~15° and ~25° of eastward tilting in the central and northern White Mountains, respectively, since the Miocene, and (2) that the White Mountains were characterized by substantial topography by ca. 4 Ma. These new $^{40}Ar/^{39}Ar$ geochronological data are summarized in Table 1, the apatite fission-track and (U-Th)He data are given in Tables 2 and 3, respectively, and sample location coordinates are listed in Table 4 (analytical procedures and $^{40}Ar/^{39}Ar$ raw data are available[1]).

Southeastern White Mountains–Cottonwood Domain

Krauskopf (1971) first described prominent, uplifted Cenozoic rhyolitic tuffs and overlying basalt flows along the eastern flank of the southern White Mountains that unconformably overlie large parts of the Cottonwood pluton (Figs. 3 and 10). Several studies correlated the rhyolitic deposits with the ca. 15 Ma Gold Coin Mine Tuff and the ca. 11.5 Ma Timber Mountain Tuff (e.g., Weiss et al., 1993; Reheis and Sawyer, 1997). Reheis and Sawyer (1997) concluded that the middle Miocene rhyolitic and basaltic sequence was deposited on a gentle erosional surface that predated Cenozoic tectonic activity. The sequence is offset by several north-trending down-to-the-west normal faults with small (<100 m) displacements (Fig. 3). Structural reconstruction of these faults suggests that the volcanic rocks overlie a very uniform, low-relief pre-Miocene erosional surface. This depositional environment is in stark contrast with that during the late Miocene and Pliocene, which was dominated by alluvial fans and substantial topographic relief (Reheis and Sawyer, 1997; this study). At present, the middle Miocene erosional surface dips ~12°–17° to the east, suggesting on average ~15° of eastward tilt of the southern White Mountains fault block since ca. 11.5 Ma (Fig. 4).

Indian Creek–Davis Mountain Domain

Detailed mapping and radiometric dating of the volcanic stratigraphy in the Indian Creek–Davis Mountain area (Figs. 8 and 10) reveal that the volcanic sequences beneath the massive, capping Davis Mountain Andesite record the entire late Cenozoic tilting history of the northern White Mountains. In the drainage north of Indian Creek and south of Davis Mountain (Fig. 8), Mesozoic igneous and metasedimentary basement is unconformably overlain by fine-grained tuffaceous sandstone and siltstone that dip uniformly to the east (~085°) at an average of ~25° (n = 18). Paleocurrent indicators in these basal sedimentary rocks point to a southeastward transport direction. The fine-grained clastic sedimentary

[1]GSA Data Repository item 2003094, $^{40}Ar/^{39}Ar$ analytical procedures and data tables, is available on the Web at http://www.geosociety.org/pubs/ft2003.htm. Requests may also be sent to editing@geosociety.org.

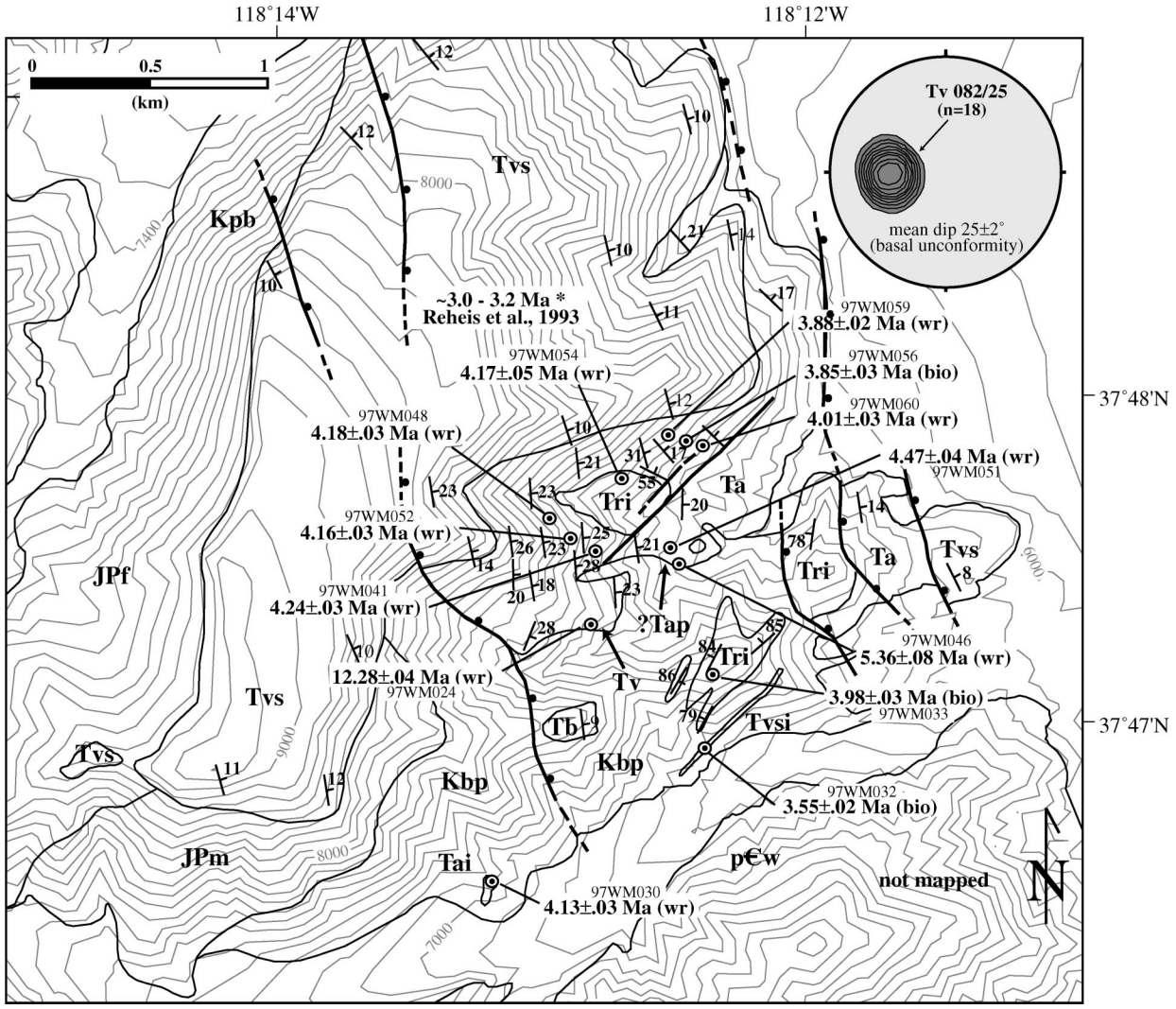

Figure 8. Geologic map of the Indian Creek–Davis Mountain area showing new $^{40}Ar/^{39}Ar$ ages from Cenozoic volcanic units along the eastern flank of the northern White Mountains (Fig. 2). For legend, see Figure 9. Bedrock geology modified after Robinson and Crowder (1973). For detailed description of Pleistocene and younger alluvial deposits and faulting, see Reheis et al. (1993). $^{40}Ar/^{39}Ar$ ages are mean weighted plateau ages, and errors are ±1σ including uncertainty in *J* (Table 1). Analyzed mineral is given in parenthesis (bio = biotite, wr = whole rock). Age estimate of Davis Mountain Andesite (Tvs) is based on K/Ar reported by Reheis et al. (1993). For simplicity, units Tv and ?Tap are not shown on map as individual unit (arrows at base of Ta). Lower-hemisphere, equal-area stereographic plot shows contoured (contour interval 3×) poles to bedding of unit Tv (ca. 12 Ma) that unconformably overlies the Mesozoic basement. Contour interval is 100 ft (~30 m).

rocks are overlain by olivine-rich basalt that yielded a $^{40}Ar/^{39}Ar$ plateau age of 12.28 ± 0.04 Ma (Fig. 8). The basal unconformity is assumed to be a valid paleohorizontal reference datum, and thus its present attitude and dip record the total tilt of the northern White Mountains since deposition of the unit at or before ca. 12 Ma. Taylor (1963) correlated similar fine-grained volcaniclastic sedimentary rocks from the area south of Montgomery Pass with the extensional middle Miocene Esmeralda Formation that is exposed across Fish Lake Valley in the Silver Peak region (Robinson et al., 1968).

The basal sedimentary and basaltic unit (Tv) is in turn unconformably overlain by a 20–30-m-thick package of andesitic tuffaceous sandstone and conglomerate (Figs. 8 and 10). An elongate, volcanic bomb–like andesite clast from the unit yielded a $^{40}Ar/^{39}Ar$ plateau age of 5.36 ± 0.08 Ma, suggesting that the unit represents a more distal equivalent of the map unit Tap in the Chiatovich area discussed in the next section (Fig. 9). The andesite is overlain by an ~150-m-thick sequence of basaltic andesite flows and tuffaceous sandstone and conglomerate composed of andesitic detritus (the lower part of Robinson and Crowder's [1973] map unit Ta). $^{40}Ar/^{39}Ar$ plateau ages for six whole-rock separates from unit Ta range from 4.47 ± 0.04 Ma near the base to 4.18 ± 0.03 Ma in the upper part of the sequence (Fig. 10). These volcanic flows dip ~15°–20° toward the northeast. However, locally these andesitic flows and tuffaceous sandstones are strongly tilted (up to 70°) around a rhyolite plug (Tri), which yielded a 4.17 ± 0.05 Ma age (Fig. 8). The intruded and tilted andesitic flows and tuffaceous sedimentary rocks are unconformably overlain by a sequence of two ~50-m-thick, massive olivine basalt units (4.01 ±

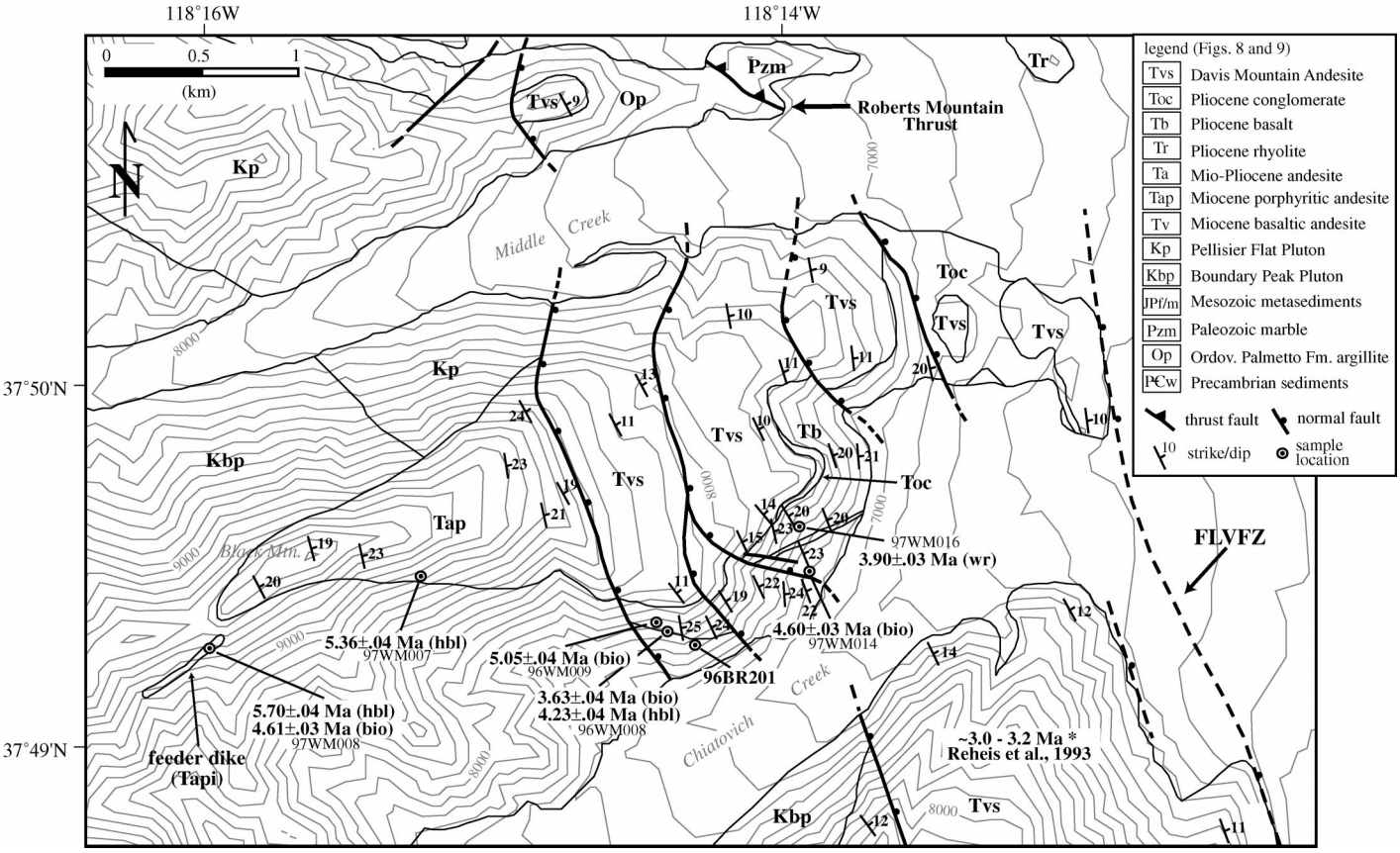

Figure 9. Geologic map of the Black Mountain–Chiatovich Creek area (Fig. 2) showing location of new $^{40}Ar/^{39}Ar$ ages from Cenozoic volcanic units along the eastern flank of the northern White Mountains; FLVFZ—Fish Lake Valley fault zone. Bedrock geology modified after Robinson and Crowder (1973). Suffix i denotes intrusive equivalent or feeder dike to same depositional unit. For detailed description of Pleistocene and younger alluvial deposits and faulting, see Reheis et al. (1993). $^{40}Ar/^{39}Ar$ ages are weighted mean plateau ages, and errors are ±1σ including uncertainty in *J*. Contour interval is 100 ft (~30 m).

0.03 and 3.88 ± 0.02 Ma) that are separated by an ~15-m-thick, partly welded rhyolite tuff (Tr) that yielded an age of 3.96 ± 0.23 Ma (Fig. 10). The angular unconformity between the deformed andesite and tuffaceous sandstone and the overlying bimodal sequence indicates that the latter postdates the diapiric emplacement of the rhyolite dome (Fig. 8). The olivine basalt flows thus appear to be equivalents to unit Tb in the Chiatovich Creek area (discussed in the next section) and to a capping basalt (Tb) along the north side of Indian Creek.

The westernmost extents of the Ta and Tb map units are controlled by a northwest-trending, down-to-the-east normal fault that juxtaposes the Pliocene volcanic sequence against Cretaceous Boundary Peak granite (Fig. 8). The bimodal sequence (Tb and Tr) is in turn unconformably overlain by up to 250 m of Pliocene Davis Mountain Andesite (Figs. 8 and 10). The fault displacement is greatly reduced at the base of the overlying Davis Mountain Andesite, suggesting that most faulting occurred in the middle Pliocene during the deposition of Ta and Tb. Reheis and Sawyer (1997) reported K/Ar ages for the Davis Mountain Andesite of 3.2–3.0 Ma.

Along the northern side of Indian Creek (Fig. 8), the Cretaceous Boundary Peak pluton is intruded by a northeast-striking vertical andesitic dike, dated at 3.55 ± 0.02 Ma. The age and composition suggest that the dike is a feeder dike of the Davis Mountain Andesite. In addition to the Davis Mountain feeder dike, a small basaltic vent is present (4.13 ± 0.03 Ma), as well as several rhyolite intrusions (Figs. 8 and 10).

Chiatovich Creek–Black Mountain Domain

In the area north of Chiatovich Creek (Figs. 2 and 9) an ~500-m-thick sequence of east-dipping andesitic to basaltic volcanic rocks rests unconformably on the middle Cretaceous Pellisier Flat and Late Cretaceous Boundary Peak plutons (Crowder et al., 1973; Hanson, 1997). The lowest part of the sequence consists of at least 150 m of thick, light gray, porphyritic hornblende andesite directly overlying basement rocks (Tap map unit of Robinson and Crowder, 1973). $^{40}Ar/^{39}Ar$ laser total-fusion ages of biotite and plateau ages of hornblende and biotite range from 5.36 ± 0.04 Ma near the base of the unit to 4.60 ± 0.03 Ma at the top of the unit (Figs. 9 and 10). The basal contact of unit Tap dips up to 20° toward the east and is characterized by abundant basal traction structures and folded flow banding, indicative of eastward flow. The unit appears to have erupted from a near-vertical, petrologically identical feeder dike (Tapi) west of Black Mountain (Fig. 9). The andesite feeder dike yielded $^{40}Ar/^{39}Ar$ plateau ages of 5.70 ± 0.04 Ma for hornblende and 4.61 ± 0.03 Ma for biotite. As no porphyritic andesite was found at higher elevations to the west of the feeder dike (Fig. 9), it seems very

likely that Tap erupted from the feeder dike and flowed down a preexisting paleoslope and should not be used as a paleohorizontal datum to constrain the tilt history.

The porphyritic andesite is overlain by a massive, up to 100-m-thick basalt unit (Tb of Robinson and Crowder, 1973). Tb is characterized by a fine-grained groundmass with <10% phenocrysts of olivine and plagioclase, yielding a $^{40}Ar/^{39}Ar$ age of 3.90 ± 0.03 Ma (Figs. 9 and 10). The entire volcanic sequence is capped by the Pliocene Davis Mountain Andesite (QTa of Robinson and Crowder, 1973; and Tvs of Reheis et al., 1993) dated at 3.2–3.0 Ma as discussed previously (Fig. 10).

In the Black Mountain area, the thickness of Tb appears to be controlled by north-trending faults with normal apparent offset (Fig. 9). The inception of faulting postdates the deposition of Tap, and individual faults exhibit greatly reduced dip-slip displacements at the lower contact of the Davis Mountain Andesite (Tvs), implying predominantly Pliocene displacement. Several studies (Reheis et al., 1993; Reheis and Sawyer, 1997) suggested that Pliocene basalts and basaltic andesites erupted during motion along northwest-trending faults of the Fish Lake Valley fault zone. In the area to the north of lower Chiatovich Creek, Davis Mountain Andesite is downdropped to the east along a north-trending fault and truncated by the Fish Lake Valley fault zone along the range front (Fig. 9). On the basis of well data, Reheis and Sawyer (1997) estimated that the minimum total displacement along the fault zone is ~600 m. North of Middle Creek, the Davis Mountain Andesite extends to the valley floor with no apparent vertical offset along the range front (Fig. 9; Reheis and Sawyer, 1997; this study). Quaternary fault scarps in alluvial-fan surfaces east of Chiatovich Creek suggest that faulting has stepped eastward through time (Reheis et al., 1993).

Along the northern side of Chiatovich Creek, a coarse conglomerate with granitic boulders (Toc) is preserved in an ~40-m-wide paleochannel (Fig. 9). The coarse-clastic conglomerate overlies a basaltic flow at the top of unit Tb (3.90 ± 0.03 Ma) and is overlain by the Davis Mountain Andesite (Tvs) (Fig. 10). The granitic boulders range in size from 50 cm to 150 cm and are poorly sorted and subangular; they appear to have been derived exclusively from the Cretaceous Pellisier Flat and Boundary Peak plutons. Reheis et al. (1993) described a paleovalley south of Indian Creek infilled by Pliocene Davis Mountain Andesite. Together these observations indicate that the northern White Mountains were characterized by substantial topography and were probably already near their present-day elevation at ca. 4 Ma.

TABLE 1. $^{40}Ar/^{39}Ar$ GEOCHRONOLOGY DATA FROM THE EASTERN WHITE MOUNTAINS

Sample number	Unit	Type	Mass (mg)	RF/L	TFA (Ma) ± 1σ	WMPA (Ma) ± 1σ	ISO (Ma) ± 1σ	MSWD	$^{40}Ar/^{36}Ar$ (atm = 295.5)
Indian Creek–Davis Mountain area									
97WM024	Tv	wr	21.7	RF	12.22 ± 0.05	12.28 ± 0.04	12.38 ± 0.08	15.91	292.1 ± 2.5
97WM030	Tai	wr	21.8	RF	4.72 ± 0.25	4.13 ± 0.03	4.17 ± 0.05	1.21	292.0 ± 3.9
97WM032	Tvsi	bio	10.2	RF	3.71 ± 0.12	3.55 ± 0.02	3.55 ± 0.04	3.71	294.8 ± 3.0
97WM033	Tr	bio	14.0	RF	3.92 ± 0.05	3.98 ± 0.03	4.00 ± 0.03	2.43	294.3 ± 1.2
97WM041	Ta	wr	35.1	RF	4.01 ± 0.11	4.24 ± 0.03	4.21 ± 0.08	18.80	295.7 ± 8.9
97WM046	Tap?	wr	18.4	RF	6.25 ± 0.64	5.36 ± 0.08	5.37 ± 0.19	1.34	295.2 ± 5.0
97WM048	Ta	wr	25.5	RF	4.58 ± 0.29	4.18 ± 0.03	4.17 ± 0.05	1.91	296.6 ± 3.3
97WM051	Ta	wr	32.5	RF	—	4.47 ± 0.04	4.48 ± 0.11	5.22	294.6 ± 13.5
97WM052	Ta	wr	23.6	RF	4.38 ± 0.22	4.16 ± 0.03	4.14 ± 0.05	3.62	299.4 ± 5.1
97WM054	Tri	bio	2.6	RF	4.19 ± 0.07	4.17 ± 0.05	4.21 ± 0.30	1.33	291.0 ± 2.5
97WM056	Tr	bio	17.1	RF	3.44 ± 0.04	3.85 ± 0.03	3.96 ± 0.23	0.26	294.1 ± 1.5
97WM059	Tb	wr	22.2	RF	3.97 ± 0.05	3.88 ± 0.02	3.88 ± 0.03	0.91	294.1 ± 3.6
97WM060	Tb	wr	21.4	RF	3.28 ± 0.23	4.01 ± 0.03	4.01 ± 0.39	260.60	291.3 ± 69.7
Chiatovich Creek–Black Mountain area									
96WM008	Tap	hbl	4.5	RF	4.20 ± 0.04	4.23 ± 0.04	4.23 ± 0.14	3.31	295.6 ± 12.8
96WM008	Tap	bio	4.5	L	3.77 ± 0.06	3.63 ± 0.04	3.70 ± 0.71	20.35	294.3 ± 22.0
96WM009	Tap	bio	4.5	RF	5.00 ± 0.02	5.05 ± 0.02	4.98 ± 0.14	1.46	299.1 ± 7.2
97WM007	Tap	hbl	12.9	RF	5.37 ± 0.04	5.36 ± 0.04	5.42 ± 0.05	1.18	291.2 ± 2.5
97WM008	Tapi	hbl	26.0	RF	5.47 ± 0.07	5.70 ± 0.04	5.67 ± 0.06	0.20	297.2 ± 0.9
97WM008	Tapi	bio	13.2	RF	4.75 ± 0.14	4.61 ± 0.03	4.61 ± 0.03	2.06	295.0 ± 1.7
97WM014	Tap	bio	11.2	RF	4.42 ± 0.11	4.60 ± 0.03	4.58 ± 0.07	9.76	300.0 ± 9.4
97WM016	Tb	wr	27.5	RF	4.53 ± 0.26	3.90 ± 0.03	3.92 ± 0.03	3.68	291.1 ± 3.2

Notes: Units and sample locations shown in Figures 8 and 9. For analytical data and procedures, Table DR1 (see text footnote 1). Abbreviations are hbl—hornblende, bio—biotite, and wr—basalt whole rock analysis. RF—resistance furnace, L—laser analysis, TFA—total fusion age, WMPA—weighted mean plateau age, ISO—inverse isochron age, MSWD—mean square of weighted deviates. In figures and interpretation of data, WMPA was used (unless otherwise stated) for resistance furnace; step-heating experiments and the TFA were used for laser analysis. See Table 4 for sample location coordinates.

FAULT-BLOCK TILT RECONSTRUCTION AND PALEODEPTH ESTIMATES

Estimates of preextensional paleodepths of rock samples in the White Mountains fault block are essential for the proper interpretation and reconstruction of the thermal structure of the crust on the basis of thermochronological data. Early and middle Miocene volcanic and sedimentary rocks that unconformably overlie basement along the eastern flank of the White Mountains suggest that little to no topographic relief existed during the time span of their deposition. Therefore, middle Miocene rhyolite and basalt predate tectonism related to the uplift of the White Mountains and faulting in Fish Lake Valley (Reheis and Sawyer, 1997). The middle Miocene basal unconformity dips ~15° toward the east in the southern White Mountains and ~25° in the northern White Mountains (Fig. 4). These data suggest that the total amount of uplift and eastward tilt of the range increases from south to north and does not decrease, as suggested by Taylor (1963). Consequently, the total displacement along the White Mountains fault zone is expected to increase from south to north as well. If a rigid, internally intact White Mountains fault block is assumed, an eastward tilt of ~25° in the north and ~15° in the south would result in normal displacement along the White Mountains fault zone of ~8 km and ~6 km, respectively. This estimate is based on the normal offset of the extrapolated preextensional Miocene unconformity across the fault block (Fig. 4). As the preextensional Miocene unconformity is buried by an estimated ~1 km of basin fill west of the fault zone in the Benton area (Russell, 1977), the total offset of this surface across the fault zone is ~8 km (Fig. 4). Similarly, a maximum of 2 km of sediment in the basin adjacent to the southern and central White Mountains (Russell, 1977) results in a total normal offset of ~6 km across the fault zone since the middle Miocene. These values are maximum fault-offset estimates, as the exact position of the preextensional Miocene unconformity below the younger basin fill and the amount of erosional downcutting below the original Miocene basal unconformity west of the White Mountains fault zone are not known.

Previous workers (e.g., Lueddecke et al., 1998) argued that the timing and magnitude of uplift and tilting of the White Mountains were constrained by uplifted late Pliocene (ca. 3 Ma) basaltic to andesitic flows, such as the Davis Mountains Andesite. However, the ge-

TABLE 2. APATITE FISSION TRACK DATA FROM THE WHITE MOUNTAINS

Sample	Elevation (m)	Number (xls)	ρ_d	Nd	ρ_s	*N*s	ρ_i	N_i	U (ppm)	AFT age (Ma) ± 1σ	$P(\chi^2)$	Mean track length (μm) ± 1σ (*n*)
Northern White Mountains												
95BR067	2070	40	1.781	5758	0.041	75	1.138	2412	6.5	12.1 ± 1.5	62	13.64 ± 0.22 (36)
95BR068	2060	40	1.781	5758	0.032	52	1.123	2286	10.2	12.3 ± 1.5	69	14.20 ± 0.24 (33)
96BR201	2280	40	1.622	4901	0.030	37	1.263	1542	9.7	6.9 ± 1.2	86	13.89 ± 0.19 (30)
96BR210	3020	25	1.713	5246	0.509	310	2.602	1586	19.0	59.3 ± 3.8	97	13.31 ± 0.12 (120)
96BR211	3460	25	1.713	5246	0.287	217	1.602	1214	11.0	57.5 ± 5.1	71	13.23 ± 0.21 (100)
96BR212	3680	25	1.731	5246	0.291	224	1.528	1175	21.2	58.6 ± 4.5	56	13.14 ± 0.18 (79)
96BR213	4110	25	1.731	5246	0.319	281	1.708	1504	24.3	53.5 ± 3.2	47	12.86 ± 0.14 (100)
96BR214	3780	25	1.758	5246	0.615	420	3.970	2713	28.2	51.6 ± 2.8	14	12.38 ± 0.16 (120)
96BR215	3340	25	1.758	5246	0.315	193	2.965	1819	21.1	43.3 ± 2.7	32	11.45 ± 0.17 (120)
96BR216	3030	25	1.776	5246	0.260	155	2.346	1398	16.5	35.0 ± 3.0	100	10.31 ± 0.22 (90)
96BR217	2750	25	1.776	5246	0.110	111	1.333	1350	9.4	25.9 ± 2.6	100	10.73 ± 0.21 (120)
96BR218	2380	25	1.795	5246	0.053	76	1.232	1774	8.6	13.7 ± 1.6	99	12.57 ± 0.18 (120)
97WM068	2010	40	1.754	5185	0.037	90	1.000	2454	7.1	11.8 ± 1.4	54	13.90 ± 0.32 (45)
Central White Mountains												
95BR061	3740	25	1.598	5982	1.211	758	6.420	4019	41.0	65.7 ± 3.8	57	13.77 ± 0.11 (150)
95BR062	3580	25	1.598	5982	0.782	428	4.273	2117	32.3	62.1 ± 4.2	82	13.74 ± 0.10 (150)
95BR064	1640	25	1.781	5758	0.586	625	4.691	5007	32.9	42.1 ± 2.4	18	12.31 ± 0.18 (150)
96BR202	3510	20	1.640	4901	1.972	529	9.131	2450	69.6	62.7 ± 3.1	92	13.68 ± 0.09 (150)
96BR203	3420	20	1.640	4901	1.842	700	7.666	2914	58.4	69.7 ± 3.1	97	13.72 ± 0.09 (150)
96BR204	3100	20	1.658	4901	0.483	186	2.502	963	18.9	56.8 ± 4.6	100	13.52 ± 0.11 (120)
96BR205	2790	20	1.658	4901	0.801	344	5.274	2266	39.8	44.6 ± 2.7	39	11.78 ± 0.13 (120)
96BR206	2610	20	1.676	5246	1.321	452	6.575	2250	49.0	59.7 ± 3.2	99	13.48 ± 0.10 (120)
96BR207	2380	20	1.676	5246	0.265	194	1.386	1016	10.3	56.7 ± 4.5	73	12.76 ± 0.11 (120)
96BR208	2200	20	1.695	5246	0.837	293	4.209	1473	31.0	59.7 ± 3.9	65	13.50 ± 0.13 (120)
96BR209	1860	20	1.695	5246	1.029	405	5.204	2049	38.4	59.3 ± 3.3	99	13.17 ± 0.12 (120)
Queen Valley												
95BR053	2220	40	1.754	5185	0.037	90	2.150	2454	7.1	12.1 ± 1.5	7	13.65 ± 0.27 (26)
95BR055	2200	25	1.598	5982	0.562	2333	1.000	3965	41.0	13.2 ± 1.2	36	13.50 ± 1.10 (150)
95BR056	2230	30	1.769	5185	0.286	416	6.872	9980	48.6	14.2 ± 1.0	1	11.72 ± 0.21 (150)
Blind Spring Hill (Benton Range)												
95BR041	1610	25	1.598	5982	0.562	2333	1.000	3965	20.0	55.6 ± 3.1	65	13.12 ± 0.17 (120)
95BR042	1720	25	1.598	5982	0.562	2333	1.000	3965	20.0	57.0 ± 3.8	49	13.24 ± 0.12 (120)

Notes: Abbreviations: Elevation, sample elevation; Number xls, number of individual grains dated; ρ_d, induced track density in external detector adjacent to dosimetry glass (× 10^6 tracks per square centimeter); N_d, number of tracks counted in determining rd; ρ_s, spontaneous track density (× 10^6 tracks per square centimeter); N_s, number of spontaneous tracks counted; ρ_i, induced track density in external detector (muscovite) (× 10^6 tracks per square centimeter); N_i, number of induced tracks counted; $P(\chi^2)$, χ^2 probability (Galbraith, 1981; Green, 1981). Age is the sample central fission-track age (Galbraith and Laslett, 1983) calculated by using the zeta calibration method (Hurford and Green, 1983).

The following is a summary of key laboratory procedures. Samples were analyzed by D. Stockli (zeta calibration factor = 356 ± 5 using CN5). All apatites were etched for 20 s in 5*N* nitric acid at room temperature. Grains were dated by external detector methods with muscovite detectors. The CN5 dosimetry glass was used as a neutron-flux monitor. Samples were irradiated in well-thermalized positions at the Oregon State University TRIGA reactor. External detectors were etched in 48% HF. Tracks were counted with Zeiss Axioskop microscope using 100× air objective, 1.25× tube factor, 10× eyepieces, transmitted light with supplementary reflected light as needed; external detector prints were located with Kinetek automated scanning stage (Dumitru, 1993). Only grains with c-axes subparallel to slide plane were dated. Confined track lengths were measured only in grains with c-axes subparallel to slide plane; only horizontal tracks were measured (within ±5–10°), following protocols of Laslett et al. (1982). Lengths were measured with computer digitizing tablet and drawing tube, calibrated against stage micrometer (e.g., Dumitru, 1993).

Modeling done with Monte Trax of Gallagher (1995). Summary of thermal-history modeling parameters used (1) binned track-lengths data and central fission-track age, (2) ±10% uncertainty on observed age, (3) ±0.35 μm uncertainty on mean track length, (4) ±0.5 μm uncertainty on standard deviation of track-length distribution, (5) initial track length of 16.3 μm, and (6) Durango apatite annealing model of Laslett et al. (1987). Age was modeled with generic algorithm method using 200 runs and 40 iterations. Output plots show runs that pass both length and age data at 95% confidence level.

ometry of the latest Miocene–Pliocene volcanic rocks cannot be used as a valid paleohorizontal reference datum, because rocks of this age are characterized by eastward flow-direction indicators and appear to infill pre-Pliocene paleotopography (Fig. 9). Latest Miocene and Pliocene east-directed paleodrainage systems, the presence of coarse boulder conglomerates, granitic boulder composition, flow fabrics in volcanic units, and vent and feeder-dike locations with respect to lava flows further discredit the assumption that these deposits can be used to constrain tilting of the range.

The accuracy of tilting estimates and fault-offset calculations depends on several factors, such as the magnitude of Miocene paleotopography, total thickness of the preextensional volcanic and sedimentary overburden, and uncertainties in post–12 Ma tilt estimates. Lateral continuity of Miocene basalt and rhyolite along the eastern flank of the White Mountains, their negligible thickness variations, and the geometry of the basal unconformity beneath these strata indicate a gentle erosional surface with little to no paleotopography prior to ca. 12 Ma. These preextensional deposits therefore provide a paleohorizontal reference frame for the structural reconstruction of the tilted White Mountains fault block and the estimation of individual sample paleodepths prior to extensional exhumation. An estimate of the preextensional sedimentary and volcanic overburden is given by the maximum thickness of basaltic and rhyolitic deposits overlying the Miocene basal unconformity. These units attain a total thickness of 70 ± 30 m (Fig. 10; Reheis and Sawyer, 1997). This value was added to all paleodepth estimates. In the central White Mountains the extensively developed Miocene basal unconformity dips ~15° to the east. The uncertainty in tilt is small owing to the lateral continuity of the stratified rocks in the tilt direction. The tilt estimate in the northern White Mountains is based on 18 structural measurements of the bedding in middle Miocene strata overlying the basal unconformity and indicate ~25° eastward tilting of the Northern White Mountains (Fig. 8). Paleodepth errors based on uncertainties in eastward tilt were included in the calculation of paleodepths of isotherms and paleogeothermal gradients, but are not shown on apparent age vs. paleodepth diagrams (Stockli et al., 2002).

TABLE 3. APATITE (U-Th)/HE DATA FROM THE WHITE MOUNTAINS

Sample	Elevation (m)	Unit	Mass (mg)	He (nmol/g)	U (ppm)	Th (ppm)	F_t	Raw age (Ma)	±1σ Ma	Corrected age (Ma)	±1σ Ma
Northern White Mountains											
95BR053	2220	Kbp	0.074	9.30	9.30	8.65	0.75	3.56	0.42	4.75	0.56
95BR056	2230	Kpg	0.058	0.61	25.44	15.42	0.73	3.87	0.21	5.30	0.29
95BR067	2070	Kbp	0.070	0.13	4.74	9.48	0.76	3.44	0.72	4.53	0.94
95BR067.1	2070	Kbp	0.080	0.16	5.12	8.34	0.76	4.21	0.40	5.54	0.52
95BR067.2	2070	Kbp	0.029	0.31	4.71	8.09	0.70	8.55	1.31	12.21	1.87
95BR068.2	2060	Kbp	0.105	0.21	3.54	5.95	0.79	8.03	0.70	10.16	0.88
95BR068.1	2060	Kbp	0.037	0.31	5.49	10.31	0.71	7.27	0.63	9.57	0.83
96BR201	2280	Kbp	0.044	0.61	9.69	18.58	0.72	7.98	0.57	11.09	0.79
96BR201	2280	Kbp	0.049	0.33	5.20	10.20	0.70	8.09	0.97	11.55	1.38
96BR210.1	3020	Kpg	0.074	4.68	8.68	39.38	0.73	48.07	0.84	65.85	1.16
96BR210.2	3020	Kpg	0.031	5.25	10.17	47.21	0.68	45.49	0.64	57.49	0.93
96BR211.1†	3460	Kpg	0.036	5.50	10.86	34.16	0.70	53.65	1.22	76.65	1.75
96BR211.2	3460	Kpg	0.033	3.98	10.47	39.30	0.68	37.23	0.72	54.75	1.06
96BR212.1†	3680	Kpg	0.047	5.90	9.69	38.49	0.74	57.90	1.45	77.87	1.95
96BR212.2†	3680	Kpg	0.047	4.08	7.13	28.10	0.72	54.66	1.07	75.92	1.48
96BR213.1†	4110	Kpg	0.041	6.82	13.81	50.14	0.66	49.07	0.60	71.78	0.91
96BR213.2	4110	Kpg	0.052	4.77	13.42	43.72	0.69	37.14	0.74	53.82	1.07
96BR214-A	3980	Kpg	0.032	3.87	20.11	38.62	0.66	24.49	0.59	37.11	0.90
96BR214-B	3780	Kpg	0.041	2.66	15.95	40.64	0.72	19.27	0.41	26.76	0.57
96BR215.1	3340	Kpg	0.060	1.45	13.34	24.82	0.70	14.00	0.35	20.00	0.51
96BR215.2	3340	Kpg	0.049	1.23	12.02	25.75	0.73	12.60	0.43	17.26	0.60
96BR216.1	3030	Kbp	0.044	0.84	8.82	17.51	0.70	12.06	0.48	17.22	0.69
96BR216.2	3030	Kbp	0.028	0.58	8.36	16.67	0.66	8.72	1.01	13.21	1.52
96BR217.1‡	2750	Kbp	0.068	2.94	5.16	12.47	0.72	66.79	1.46	92.76	2.03
96BR217.2‡	2750	Kbp	0.032	1.81	4.31	11.73	0.74	47.05	0.92	63.58	1.24
96BR217.3‡	2750	Kbp	0.050	1.31	4.65	12.27	0.71	32.07	1.31	45.17	1.84
96BR218.2	2380	Kbp	0.073	0.33	4.96	10.12	0.75	8.25	0.66	11.01	0.88
96BR218.1	2380	Kbp	0.058	0.39	5.79	9.83	0.74	8.96	0.82	12.11	1.11
97WM068	2010	Kpg	0.037	0.92	11.88	42.54	0.69	7.76	0.44	11.25	0.63
Central White Mountains											
95BR061	3740	Jbp	0.063	15.19	60.21	27.05	0.75	42.15	0.44	56.20	0.58
95BR062	3580	Jbp	0.048	10.36	37.37	25.77	0.73	44.04	0.74	60.33	1.01
95BR064.1	1640	Jbp	0.031	4.32	21.64	22.62	0.70	29.62	0.50	41.72	0.70
95BR064.2	1640	Jbp	0.020	4.12	19.95	23.07	0.75	29.97	0.79	39.96	1.06
96BR202	3510	Jbp	0.045	14.93	63.80	37.62	0.71	37.98	0.80	53.49	1.12
96BR203	3420	Jbp	0.057	12.12	50.60	16.83	0.73	41.05	0.54	56.24	0.74
96BR204	3100	Kma	0.031	1.52	7.35	15.27	0.69	25.61	1.05	37.12	1.52
96BR205.1	2790	Jbp	0.025	5.72	37.21	34.72	0.67	23.32	0.76	34.80	1.13
96BR205.2	2790	Jbp	0.032	6.46	39.54	33.09	0.71	25.24	0.43	36.06	0.62
96BR206.1	2610	Jbp	0.028	8.34	46.12	31.45	0.67	28.82	0.83	43.02	1.24
96BR206.2	2610	Jbp	0.033	8.19	41.24	28.22	0.70	31.62	0.45	42.17	0.64
96BR207.1	2380	Kg?	0.035	5.79	15.33	48.17	0.70	40.03	0.87	57.19	1.25
96BR207.2	2380	Kg?	0.039	3.17	9.40	40.52	0.71	30.92	0.62	53.55	0.87
96BR208.1	2200	Jbp	0.030	5.55	38.68	32.16	0.70	22.20	0.37	33.72	0.53
96BR208.2	2200	Jbp	0.050	6.09	36.00	26.34	0.72	26.70	0.40	37.09	0.56
96BR209.1	1860	Jbp	0.048	5.05	26.87	25.05	0.72	28.49	0.54	39.58	0.75
96BR209.2	1860	Jbp	0.033	5.22	39.19	31.16	0.70	20.33	0.34	39.04	0.48
Queen Valley											
95BR053	2220	Kbp	0.074	9.30	9.30	8.65	0.75	3.56	0.42	4.75	0.56
95BR055	2200	Kpg	0.052	12.60	12.60	31.48	0.80	2.90	0.08	3.64	0.10
95BR056	1980	Kpg	0.058	25.44	25.44	15.42	0.73	3.87	0.21	5.30	0.29
97WM064	2140	Kpg	0.037	14.66	14.66	36.52	0.69	1.87	0.40	2.67	0.57
97WM065	2070	Kpg	0.049	35.94	35.94	34.96	0.73	2.22	0.16	3.00	0.22
97WM066	2270	Kpg	0.033	16.68	16.68	22.59	0.70	2.84	0.51	4.12	0.74
Blind Spring Hill (Benton Range)											
95BR041.1	1610	Trg	0.049	37.29	37.29	56.13	0.71	34.49	0.72	48.58	1.01
95BR041.1	1610	Trg	0.044	37.05	37.05	58.96	0.72	35.29	0.48	49.01	0.67
95BR042	1720	Jg	0.021	31.18	31.18	63.95	0.66	33.01	0.55	50.01	0.84

Notes: (U-Th)/He data from the White Mountains area (see Fig. 12 for sample locations and Table 4 for sample coordinates). Elevation—sample elevation; unit, Kbp—Boundary Peak Granite, Kpg—Pellisier Flat Granite, Jbp—Barcroft Pluton, Kma—McAfee pluton, Kg?—Cretaceous granite, Trg—Triassic granite, and Jg—Jurassic granite; F_t—alpha ejection correction after Farley et al. (1996). The dimensions of the apatite grains in each sample (15–20 grains) were measured to determine the alpha-emission correction (Farley et al., 1996). He ages were calculated on the basis of absolute He and U-Th determinations on the same sample. For He analyses, samples were first outgassed (Wolf et al., 1996), then retrieved and dissolved in a doubly spiked (^{230}Th-^{235}U) HNO_3 solution in preparation for U and Th determinations using isotope dilution ICP-MS (inductively coupled plasma–mass spectrometry). Analyses were performed by Stockli at the California Institute of Technology in the laboratory of K. Farley. Samples are characterized by excess helium from detected inclusion (†) or from fluid inclusions (‡) and were not included in data analysis and interpretation.

APATITE FISSION-TRACK AND (U-Th)/He THERMOCHRONOLOGY

Apatite fission-track and (U-Th)/He dating methods are particularly effective tools for directly dating the footwall exhumation and cooling that accompany major normal fault slip in the brittle crust. Footwall rocks move up relative to the adjacent hanging-wall rocks during major fault slip, causing exhumation and cooling that can be directly dated. Many studies have successfully utilized this general approach of investigating the low-temperature cooling histories of normal fault–bounded crustal blocks (e.g., Foster et al., 1991, 1993; Fitzgerald et al., 1991; Gans et al., 1991; John and Foster, 1993; John and Howard, 1995; Howard and Foster, 1996; Miller et al., 1999; Reiners et al., 2000; Stockli et al., 2000, 2001, 2002).

Laboratory and natural calibration studies of preexhumation apatite fission-track and (U-Th)/He data patterns have demonstrated how apparent ages and track length vary systematically with depth and burial temperature (Green et al., 1989a; Wolf et al., 1996, 1998; Dumitru, 2000; Stockli et al., 2000). In areas where high-angle normal faults accommodate crustal extension, mountain ranges typically correspond to major tilted crustal blocks. The footwalls of such extensional faults have been exhumed from substantial depths. If fault slip has been rapid and of sufficient magnitude, (U-Th)/He and fission-track ages will directly reveal the time of exhumation. At shallower and shallower paleodepths, apparent ages are progressively older because the radiometric clocks were not completely reset to zero before exhumation commenced. These partly reset samples also retain valuable information that can be interpreted by using fission-track modeling (e.g., Green et al., 1989b; Gallagher, 1995; Ketcham et al., 2000).

A total of 51 thermochronology samples were collected from the northern and central White Mountains and Blind Spring Hill in the Benton Range (Fig. 11). Apatite from all of the samples was analyzed by the fission-track method at Stanford University, and apatite from 34 samples was analyzed by the (U-Th)/He technique at the California Institute of Technology (Tables 2, 3, and 4). Samples were collected systematically along the base of the White Mountains in the footwall of the White Mountains fault zone as well as in the Blind Spring Hill area, which is situated in the hanging wall (Figs. 2 and 11). In addition, two east-west sampling transects across the northern and central White Mountains fault block were carried out between Chiatovich Creek

TABLE 4. GEOCHRONOLOGICAL AND THERMOCHRONOLOGICAL SAMPLE LOCATIONS

Sample number	Latitude, longitude (N), (E)	Elevation (m)	PD (km)	Sample number	Latitude, longitude (N), (E)	Elevation (m)	PD (km)
95BR041	37°45′52″, 118°27′25″	1610	~2	96BR217	37°46′50″, 118°23′13″	2750	5.50
95BR042	37°49′12″, 118°30′16″	1720	~2	96BR218	37°46′51″, 118°24′20″	2380	5.70
95BR053	37°50′04″, 118°24′37″	2220	6.60	96WM008	37°49′17″, 118°14′24″	2320	v
95BR055	37°52′34″, 118°23′37″	2200	6.58	96WM009	37°49′17″, 118°14′27″	2335	v
95BR056	37°53′42″, 118°22′43″	2230	6.55	97WM007	37°49′28″, 118°15′15″	2700	v
95BR061	37°49′20″, 118°14′14″	3740	1.28	97WM008	37°49′19″, 118°16′03″	2865	v
95BR062	37°48′39″, 118°14′34″	3580	1.51	97WM014	37°49′31″, 118°14′00″	2290	v
95BR064	37°47′38″, 118°19′40″	1640	4.11	97WM016	37°49′35″, 118°14′03″	2345	v
95BR067	37°46′56″, 118°24′36″	2070	6.50	97WM024	37°47′18″, 118°12′41″	2160	v
95BR068	37°46′05″, 118°23′50″	2060	6.25	97WM030	37°46′34″, 118°13′03″	2200	v
96BR201	37°49′11″, 118°14′24″	2280	0.01	97WM032	37°46′59″, 118°12′20″	2080	v
96BR202	37°48′51″, 118°15′14″	3510	1.82	97WM033	37°47′09″, 118°12′22″	2210	v
96BR203	37°48′38″, 118°15′20″	3420	2.05	97WM041	37°47′34″, 118°12′33″	2085	v
96BR204	37°48′33″, 118°16′20″	3100	2.45	97WM046	37°47′31″, 118°12′27″	2130	v
96BR205	37°48′30″, 118°17′10″	2790	2.69	97WM048	37°47′39″, 118°12′45″	2240	v
96BR206	37°48′17″, 118°17′49″	2610	2.81	97WM051	37°47′34″, 118°12′27″	2140	v
96BR207	37°48′08″, 118°18′31″	2380	3.18	97WM052	37°47′36″, 118°12′41″	2170	v
96BR208	37°47′55″, 118°19′08″	2200	3.55	97WM054	37°47′44″, 118°12′33″	2135	v
96BR209	37°47′56″, 118°19′38″	1860	4.05	97WM056	37°47′50″, 118°12′24″	2160	v
96BR210	37°47′50″, 118°17′47″	3020	1.65	97WM059	37°47′51″, 118°12′26″	2165	v
96BR211	37°47′32″, 118°18′08″	3460	2.10	97WM060	37°47′50″, 118°12′22″	2150	v
96BR212	37°47′16″, 118°19′10″	3680	2.25	97WM064	37°57′36″, 118°20′00″	2140	n, a
96BR213	37°46′45″, 118°19′50″	4110	2.27	97WM065	37°55′52″, 118°19′56″	2070	n, a
96BR214	37°47′19″, 118°21′50″	3780	3.65	97WM066	37°53′54″, 118°21′00″	2270	n, a
96BR215	37°47′00″, 118°22′00″	3340	4.25	97WM068	37°59′30″, 118°22′20″	2010	6.50
96BR216	37°46′47″, 118°22′56″	3030	5.00				

Note: Listing of coordinates, elevations, and paleodepth estimates for $^{40}Ar/^{39}Ar$, apatite fission-track, and apatite (U-Th)/He samples. PD, calculated preextensional paleodepth; v denotes volcanic surface sample. See Figures 8, 9, and 11 for sample location maps.

and Marble Canyon and between east of Mount Barcroft and Chalfant; these transects sampled the entire upper-crustal section exposed in the White Mountains. The different systematic sample arrays were collected to constrain different aspects of the tectonic and exhumation history of the White Mountains fault block. The range-front-parallel sample array was expected to yield insights into along-strike variations in magnitude of exhumation and faulting, whereas cross-range vertical transects were designed to constrain the cooling history of the extensional fault block and to determine the timing of onset of normal faulting (Stockli et al., 2000).

All samples for this study were taken from outcrops of fresh, unaltered Mesozoic granitic rocks. Cretaceous metavolcanic rocks did not yield sufficient apatite for analysis. Thermochronological samples were collected as far as possible from exposed Cenozoic dikes and volcanic units in order to avoid thermal effects, unless otherwise stated. All apatite fission-track and (U-Th)/He analyses for individual samples were performed on aliquots of the same apatite separates. Electron-microprobe analyses of apatite ($Ca_5(PO_4)_3$[F,Cl,OH]) demonstrate that all analyzed samples are exclusively fluorapatite with very low chlorine contents of <0.15 wt% Cl in samples from the Cretaceous Boundary Peak, Pellisier Flat, and McAfee plutons and ~0.3 wt% Cl in samples from the Jurassic Barcroft pluton (Stockli et al., 2000).

Apatite Fission-Track Thermochronology

Fission tracks are linear damage trails in the crystal lattice that form as the result of spontaneous nuclear fission of trace ^{238}U (e.g., Fleischer et al., 1975; Dumitru, 2000; Gleadow et al., 2002). Use of apatite data for reconstructing cooling and unroofing histories relies on the fact that new ^{238}U fission tracks form at an essentially constant rate and with an essentially constant initial track length, whereas tracks are simultaneously annealed (erased) by elevated subsurface temperatures (Gleadow et al., 1986a; Green et al., 1989a, 1989b; Dumitru, 2000). The annealing process causes easily measured reductions in both track lengths and apparent fission-track ages (Naeser, 1979, 1981; Gleadow et al., 1986a, 1986b; Green et al., 1989a, 1989b; Crowley et al., 1991; Corrigan, 1991). At temperatures hotter than ~110–125 °C, all fission tracks are totally annealed, resetting the fission-track clock to zero. Tracks are partially annealed between ~60 °C and ~120 °C, a temperature range termed the partial annealing zone (PAZ) (Gleadow et al., 1986a; Green et al., 1989a, 1989b). Below ~60 °C, fission tracks in apatite are effectively stable, and annealing occurs only at very slow rates (Fitzgerald and Gleadow, 1990).

(U-Th)/He Thermochronology

(U-Th)/He thermochronology is based on the decay of U and Th to Pb, producing ^4He by alpha-particle emission (e.g., Zeitler et al., 1987; Farley, 2002; Reiners, 2002; Farley and Stockli, 2002). In apatite, He is essentially totally retained within the apatite crystal at temperatures below ~45 °C, entirely lost by diffusion above ~85 °C, and partly retained between ~45 and ~85 °C (e.g., Wolf et al., 1998; Stockli et al., 2000). The apatite He partial retention zone (PRZ) is conceptually similar to the PAZ of the fission-track system, and sample data can be interpreted in a similar fashion. An important complication in (U-Th)/He dating arises from the fact that during decay of U and Th, alpha particles are emitted with high kinetic energy and travel significant distances before coming to rest. In small mineral grains, considerable proportions of the alpha particles will leave the grain, resulting in an underestimation of the (U-Th)/He age. Farley et al. (1996) showed that the underestimate is a function of grain size and shape parameters and can be corrected by using a morphometric correction factor. The low-temperature cooling histories attainable through the (U-Th)/He technique allow dating of neotectonic and small-magnitude tectonic motions in the upper crust, making apatite (U-Th)/He dating a powerful complement to the apatite fission-track method.

The concept of an exhumed partial annealing or retention zone (PAZ or PRZ) can provide important constraints on the timing, rate, and magnitude of cooling and exhumation of crustal fault blocks. In addition, the lower and upper bounds of an exhumed PRZ or PAZ can serve as proxies for preextensional paleoisotherms that may be used to estimate a geothermal gradient prior to the onset of exhumation. This estimate is simply calculated by dividing the ΔT (temperature of paleoisotherm minus temperature of paleosurface) by the estimate of paleodepth of the same paleoisotherm. Furthermore, exhumed PAZs or PRZs can be used as passive structural markers that, when offset across fault zones, can constrain the magnitude of fault displacement (e.g., Fitzgerald, 1992).

Northern White Mountains

Figure 12 summarizes fission-track and (U-Th)/He ages from the east-west sampling transect across the northern White Mountains fault

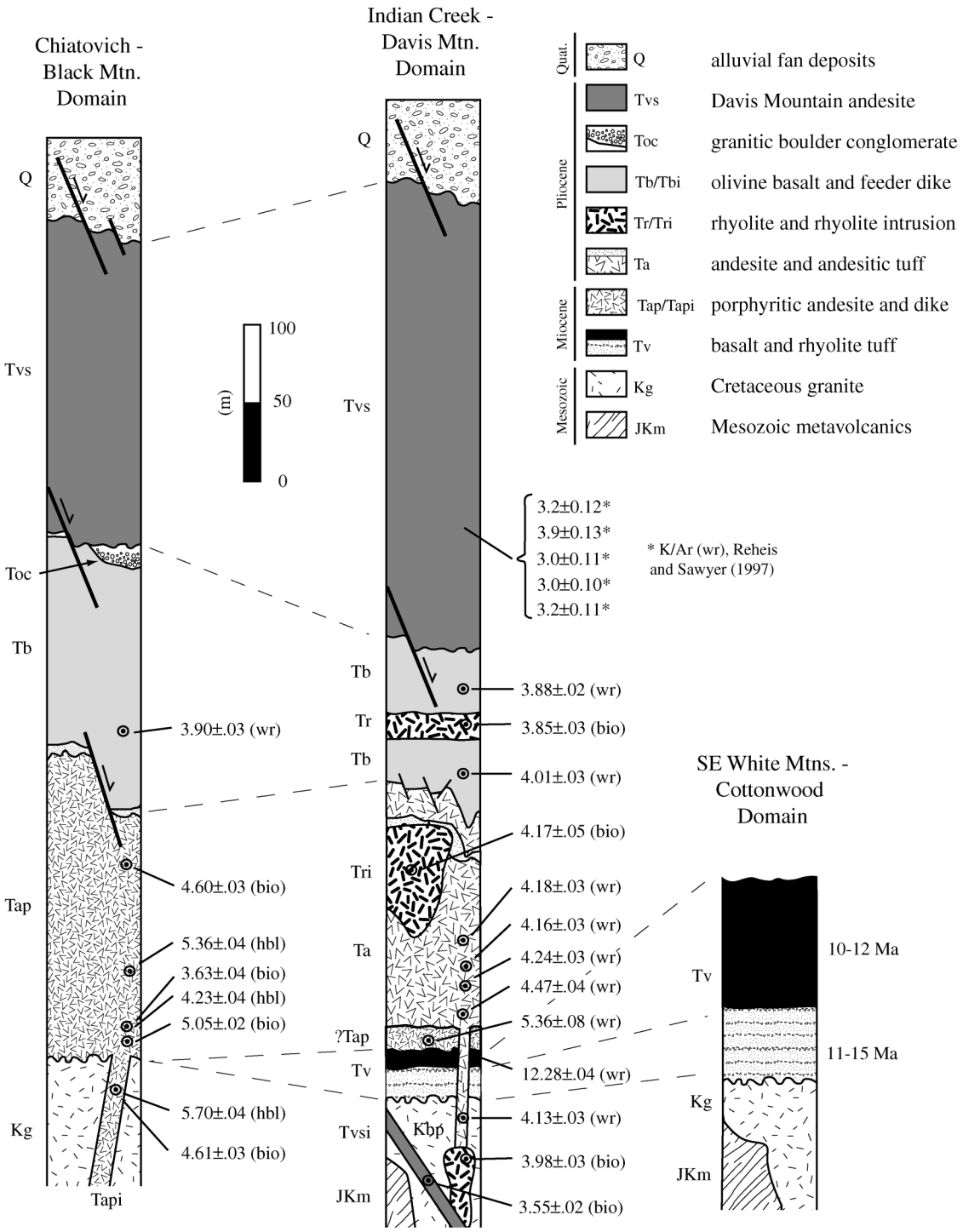

Figure 10. Schematic Cenozoic volcanic stratigraphy of the northern and central part of the eastern White Mountains. $^{40}Ar/^{39}Ar$ data are plateau ages with (±1σ) error including the uncertainty in *J*. For detailed discussion, see text and Figures 8 and 9.

block. Plots of apparent ages and track lengths vs. structural level exhibit patterns that correspond well with theoretical postexhumation apparent age vs. paleodepth trends (e.g., Fitzgerald et al., 1991; Howard and Foster, 1996; Miller et al., 1999) (Fig. 13). Fission-track and (U-Th)/He ages from structurally shallow samples cluster tightly around ca. 58 Ma and 53 Ma, respectively. The age data in combination with moderately long mean track lengths (13.2 ± 0.3 μm) are consistent with Late Cretaceous–early Tertiary cooling and/or regional exhumation of the inactive Sierra Nevada magmatic arc. One structurally shallow sample (96BR212) yielded an anomalously old (U-Th)/He age that is substantially older than the corresponding fission-track age (Table 1). This anomalous result is best explained

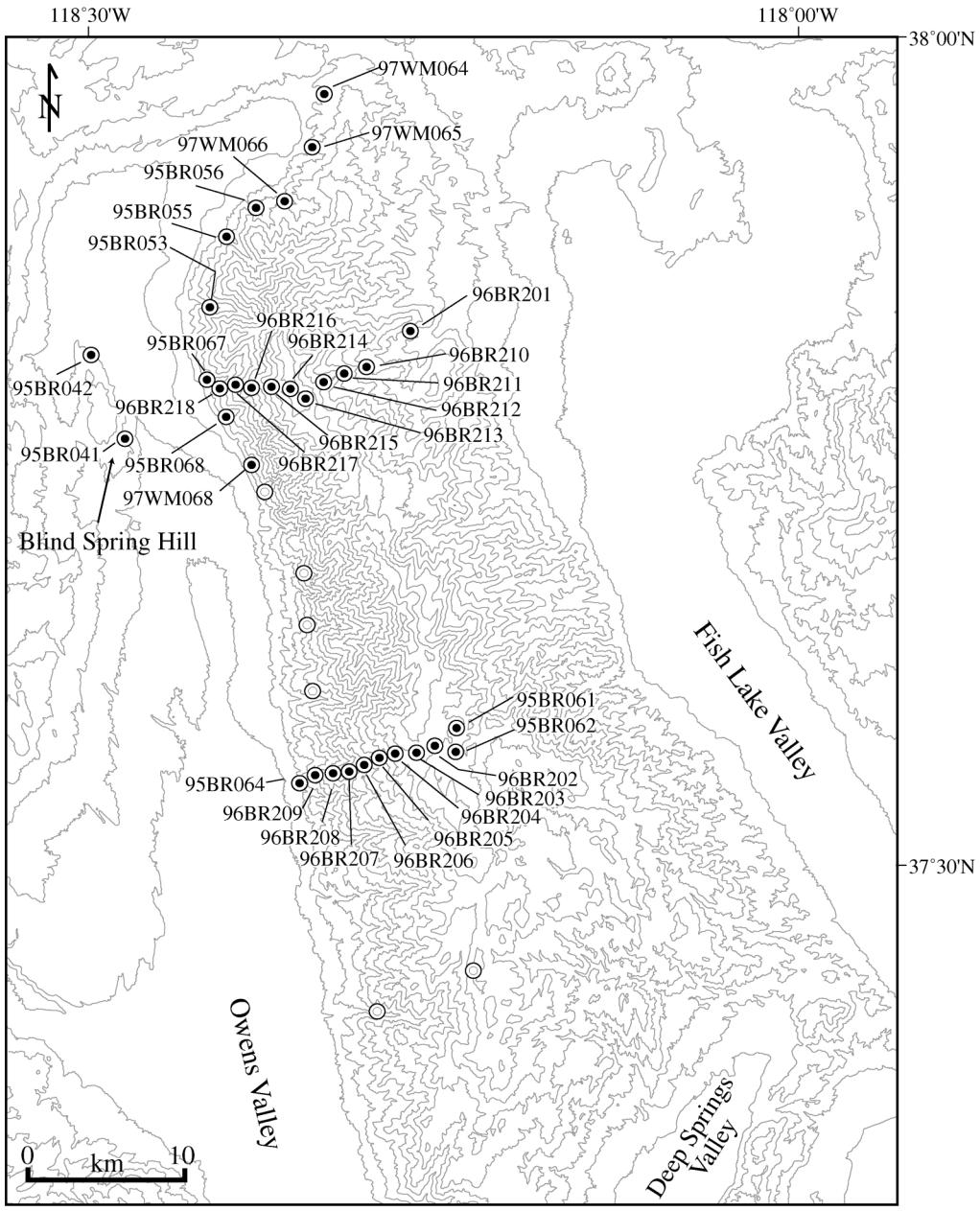

Figure 11. Topographic map of the White Mountains showing locations of samples collected for fission-track and (U-Th)/He thermochronological analysis (Tables 2, 3, and 4). Open dots with no sample numbers denote samples with insufficient apatite yields for analysis. Contour interval is 100 m. Blind Spring Hill is in the Benton Range.

by excess He parented by small U-bearing zircon inclusions (House et al., 1999; Table 3). The structurally shallowest sample (96BR201) from Chiatovich Creek yields an apatite fission-track age of 6.9 ± 1.2 Ma (Fig. 9). This sample was collected ~5 m below the Pliocene andesitic unit Tap dated at ca. 5.5 Ma, indicating that the fission-track age was fully reset as a result of reheating during the extrusion of Tap (Figs. 9 and 13). The corresponding (U-Th)/He age is ca. 11 Ma and suggests that He was not completely degassed during the brief reheating related to the emplacement of the andesite (see Stockli et al., 2000).

Below a paleodepth of ~3 km, apparent apatite fission-track ages systematically decrease with increasing preextensional paleodepths, ranging from 59.3 ± 3.8 Ma at ~3 km paleodepth to 13.7 ± 1.6 Ma at ~6.2 km (Fig. 13; Tables 2 and 3). These samples define a well-behaved exhumed apatite fission-track PAZ, which is also corroborated by the track-length data (Fig. 13). The samples from the PAZ display unimodal, slightly negatively skewed track-length distributions that are characterized by progressively shorter mean track lengths with increasing paleodepth, indicative of increasing degrees of annealing, whereas samples from below the base of the PAZ are characterized by long mean track lengths (Fig. 13). At paleodepths of ~6.2 ± 0.5 km, a major inflection occurs in the fission-track apparent age vs. paleodepth curve; the inflection defines the base of an exhumed preextensional Miocene PAZ (Fig. 13). The base of the PAZ

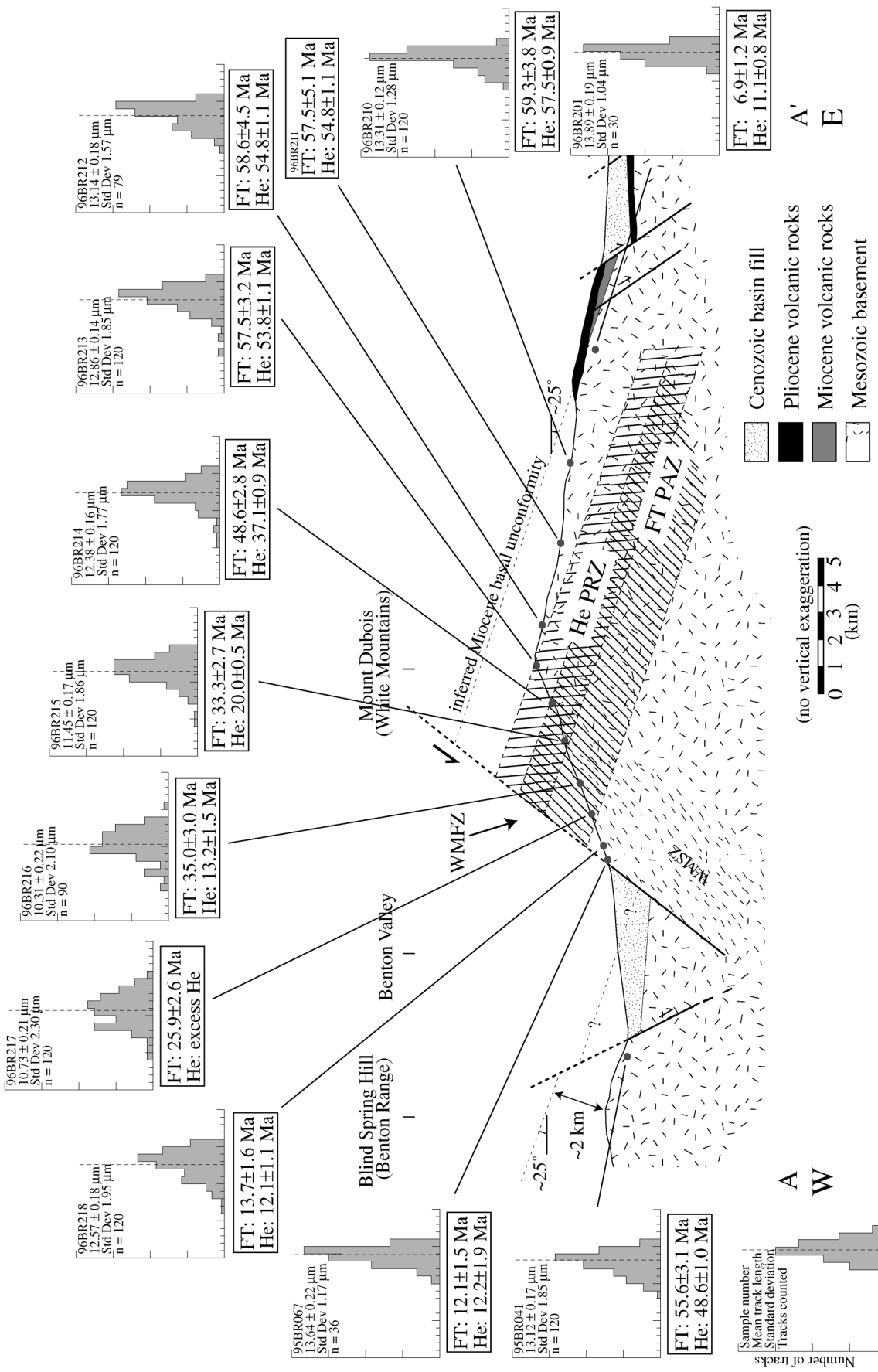

Figure 12. Schematic cross section of the northern White Mountains and Blind Spring Hill area in the Benton Range, showing apatite fission-track age and length data (top values in boxes) and (U-Th)/He age data (bottom values in boxes) from along cross-sectional trace. Geometry of apatite fission-track partial annealing zone (FT PAZ) and (U-Th)/He partial retention zone (He PRZ) are based on fault kinematic data and structural reconstructions of the preextensional configuration of Miocene volcanic rocks along the eastern flank of the northern White Mountains. Depth below Miocene unconformity in Blind Spring Hill area is estimated on the basis of thermochronological constraints. See Figures 2 and 11 for location.

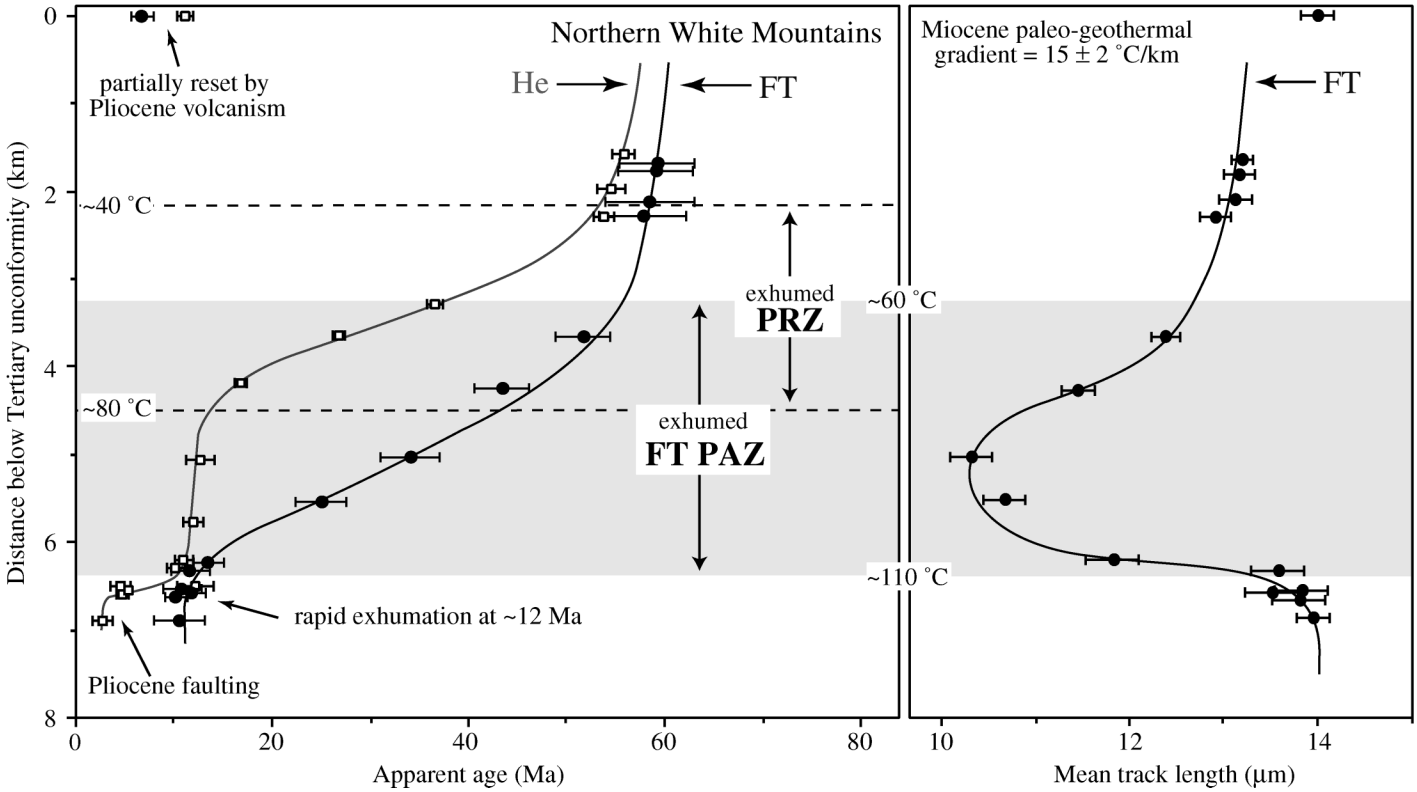

Figure 13. Plot of apatite fission-track and (U-Th)/He data vs. preextensional structural depth from the northern White Mountains. Concordant fission-track and (U-Th)/He ages and invariant cooling ages below the base of the PAZ and PRZ indicate rapid cooling and exhumation of the White Mountains starting at ca. 12 Ma. Younger (U-Th)/He ages at the base of the northern White Mountains reflect renewed exhumation as a result of Pliocene transtensional faulting and the formation of the Queen Valley pull-apart structure. Apatite fission-track mean track lengths define an exhumed Miocene PAZ that is characterized by a well-defined base marking the position of the preextensional middle Miocene ~110 °C isotherm. The top of the PAZ is less well defined because of the gradually increasing degree of annealing of Late Cretaceous to early Tertiary cooling ages. The depths to the bases of the PAZ and the PRZ yield consistent preextensional geothermal-gradient estimates of 15 ± 2 °C/km. The continuous nature of the age vs. depth behavior also underlines the absence of faults within the northern White Mountains footwall.

is also evident from the mean fission-track lengths that increase from 10.7 ± 0.2 μm above the base of the PAZ to 13.9 ± 0.3 μm below. The (U-Th)/He age data also exhibit a well-defined PRZ characterized by a decrease in apparent age with increasing depth from 53.8 ± 1.1 Ma at ~2.3 km paleodepth to 17.2 ± 0.7 Ma just above the base of the PRZ at ~4.5 km (Fig. 13).

Samples from below the PAZ and PRZ are characterized by concordant cooling ages and long mean track lengths that are invariant with depth (Fig. 13). The concordance of fission-track and (U-Th)/He ages indicates that rocks from the base of the range cooled very rapidly from >120 °C to <40 °C at ca. 12 Ma. Given the estimated middle Miocene paleogeothermal gradient of ~15 °C/km (Fig. 13), the rapid cooling of these rocks (>80 °C) indicates that the White Mountains fault block was exhumed by at least 4.5 km at ca. 12 Ma. This value is a minimum estimate, and the samples could have cooled to temperatures well below 40 °C at ca. 12 Ma, indicating even greater exhumation and fault slip along the White Mountains fault zone.

The structurally deepest sample (95BR067) along the western range front of the northern White Mountains is characterized by mean track lengths of ~13.9 μm, suggesting that this sample resided immediately below the base of the PAZ at temperatures of ~120 °C prior to Miocene faulting (Fig. 13). The rapid cooling to temperatures of <40 °C at ca. 12 Ma also implies that subsequent Pliocene normal displacement along the White Mountains fault zone must have been of limited magnitude (<1–1.5 km).

Central White Mountains

Samples were collected from the Jurassic Barcroft and Cretaceous McAfee plutons along the crest of the White Mountains from White Mountain Peak to Mount Barcroft and from Mount Barcroft down to the range front east of Chalfant (Fig. 6). Structurally shallow samples yield apatite fission-track and (U-Th)/He ages ranging from 70 to 62 Ma and from 60 to 53 Ma, respectively (Figs. 14 and 15; Tables 2, 3, and 4). The age and track-length data (mean lengths of ~12.5–13 μm) suggest a Late Cretaceous to early Tertiary cooling episode similar to that discussed in the previous section for the northern White Mountains (Fig. 13). As was documented by geologic mapping and fault kinematic data (Figs. 5 and 6), the White Mountains fault zone in the central White Mountains consists of four parallel normal faults that progressively down-drop the hanging wall in a step-like fashion with respect to the footwall (Fig. 15). As a consequence of the down-dropped fault blocks along the western range front, the bases of the fission-track PAZ and (U-Th)/He PRZ are not exposed, and the timing

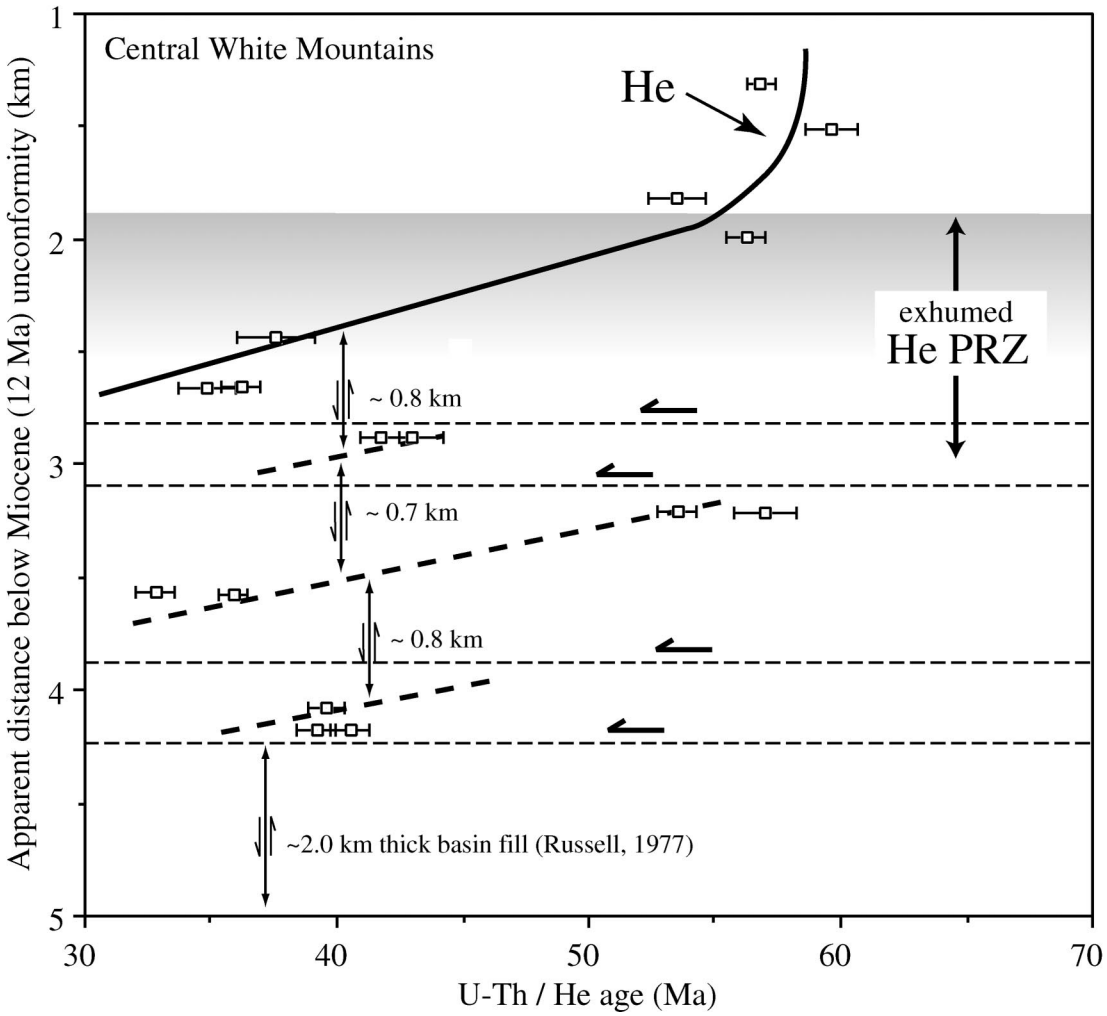

Figure 14. Plot showing apparent (U-Th)/He ages vs. distance below Miocene unconformity in the central White Mountains. The central White Mountains fault zone consists of four structurally defined normal-fault zones that progressively down-dropped fault slivers to the west (Figs. 6 and 15). Structural duplication and offsets in the (U-Th)/He apparent age vs. paleodepth pattern illustrate the down-to-the-west normal faulting and allow the estimation of fault offset across individual normal faults using the preextensional thermal state within the crustal fault block as a structural marker. The technique does not yield precise fault-displacement estimates, but the cumulative fault-offset estimates are in good agreement with the total offset across the White Mountains fault zone based on the structural reconstruction of the central White Mountains using tilted Miocene basalts. Fault offsets calculated from offsets in the PRZ are based on an ~60° dipping normal fault.

of inception of faulting cannot be dated directly.

The lack of offset geologic markers makes it difficult to assess the fault-normal displacement across the individual faults. However, the repetition of part of the PRZ and actual offsets in the (U-Th)/He age vs. paleodepth profile allow the estimation of fault displacement across individual normal faults (Fig. 14). This is a well-established approach to quantify the magnitude of fault displacement by using fission-track data (e.g., Fitzgerald, 1992, 1994; Foster and Gleadow, 1996; Kamp, 1997). Figures 14 and 15 illustrate this technique by using the (U-Th)/He data from the central White Mountains. The (U-Th)/He age vs. paleodepth profile is systematically offset across the normal faults, juxtaposing older apparent ages in the hanging wall with younger ages in the footwall (Fig. 14). Figure 15 shows a similar behavior for the fission-track data. Based on the thermochronological data, the three major normal faults within the range in the central White Mountains accommodate ~2.5 km of cumulative normal displacement. The minimum displacement along the range-bounding fault is estimated at ~2.0 km on the basis of the thickness of the hanging-wall basin fill near Chalfant of ~2 km (Russell, 1977). The total cumulative offset derived from (U-Th)/He data and basin-fill thickness suggests a total Cenozoic normal displacement of ~4.5 km (Fig. 15). However, the total Cenozoic normal offset across the White Mountains fault zone in the central White Mountains is ~6 km according to a structural reconstruction of tilted basalt flows along the eastern flank of the central White Mountains, implying that, in total, ~3.5 km of normal-fault displacement was accommodated by faults along the range front (Fig. 4).

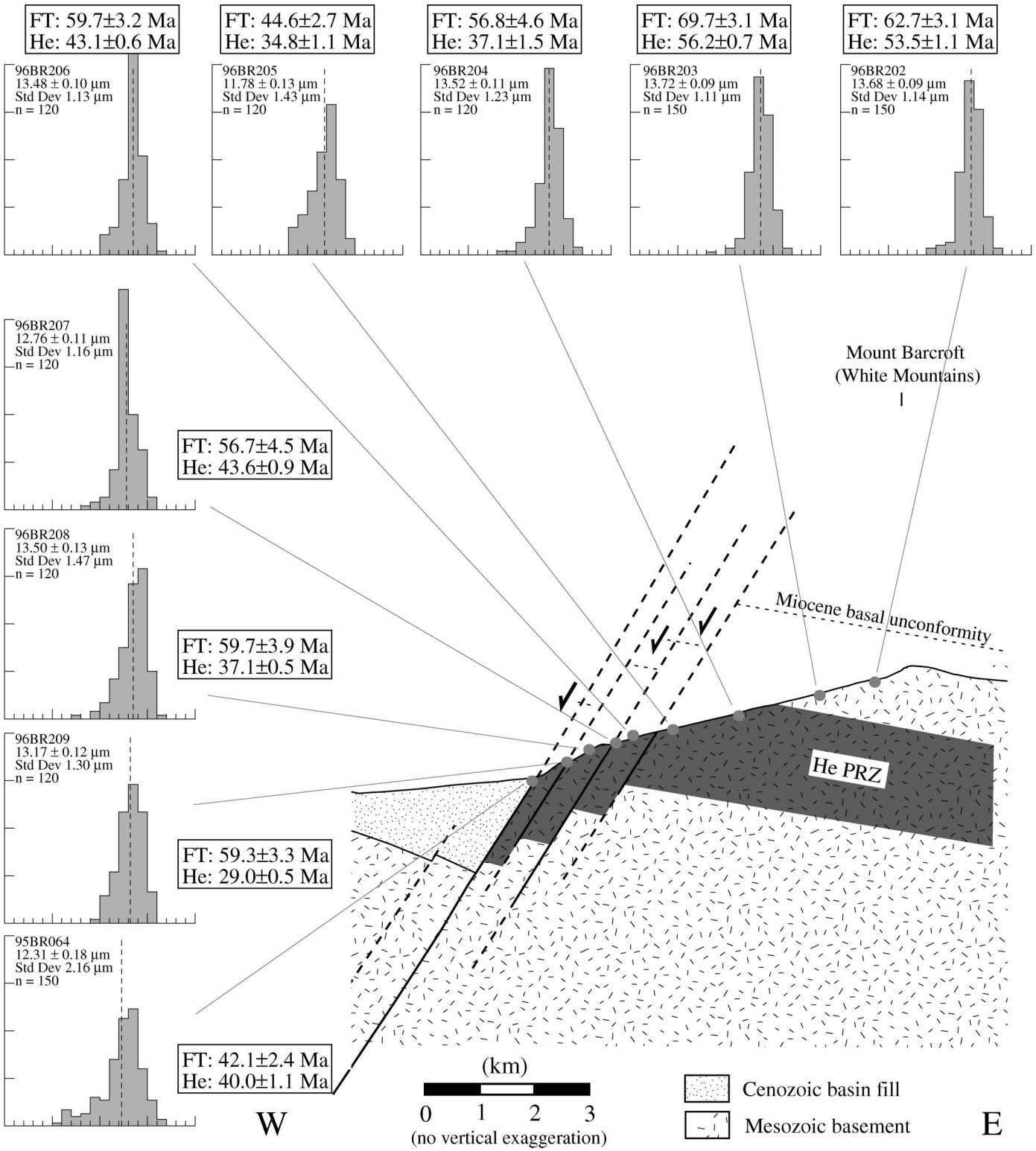

Figure 15. Simplified cross section of the western range front in the central White Mountains (Fig. 3) showing apatite fission-track and (U/Th)/He ages and distributions of fission-track lengths. The White Mountains fault zone consists of four major, parallel normal faults that progressively down-dropped fault slivers to the west as indicated by the offset (U-Th)/He PRZ. Within individual fault blocks, apparent ages and mean track lengths decrease with decreasing elevation and paleodepth. Offsets in apparent ages vs. paleodepth profiles and mean track-length pattern document normal displacements across individual, structurally defined normal faults. Fault offsets juxtapose longer mean track lengths in the hanging wall with significantly shorter mean track lengths in the footwall.

Blind Spring Hill in the Benton Range

Basement rocks similar to those in the northern White Mountains are present in the Benton Range in the hanging wall of the White Mountains fault zone. Two samples yield apatite fission-track ages of ca. 56 and ca. 57 Ma, whereas the corresponding (U-Th)/He apparent ages are ca. 50–49 Ma (Fig. 12; Tables 2, 3 and 4). These data suggest that rocks in the hanging wall of the fault zone underwent a cooling history similar to samples from structurally shallow levels in the footwall of the fault zone along the crest and the eastern flank of the northern White Mountains. Apatite fission-track and U-Th/He ages for basement samples in the Benton Range (95BR041 and 95BR042) are most similar to those for sample 96BR213 in the White Mountains east of the fault zone, suggesting that these samples were all at a similar depth (~2 km) below the Miocene basal unconformity prior to 12 Ma (Fig. 12). If one assumes a 25° eastward dip of the unconformity in the Benton Range, offset of this surface across the White Mountains fault zone is ~8–9 km, depending on the amount of displacement on the east-dipping normal fault along the eastern side of Blind Spring Hill. This estimate is in excellent agreement with structurally derived constraints for the normal displacement across the White Mountains fault zone (see earlier section in this paper).

Queen Valley Pull-Apart Structure

Structural data from the area north of Marble Canyon indicate that late-stage northwest-southeast extension resulted in renewed uplift of the White Mountains and formation of the Queen Valley pull-apart basin (Figs. 2 and 16). The deepest structural levels in this part of the White Mountains are characterized by younger (U-Th)/He ages of ca. 3–5 Ma (Fig. 16), recording a renewed phase of cooling and exhumation in Pliocene time. Samples from Queen Valley, Montgomery Canyon, and the base of Marble Canyon yielded apparent (U-Th)/He ages that decrease with decreasing elevation and exhibit an inflection point at ~2200 m, suggesting the existence of an exhumed Pliocene PRZ. The concordant and invariant ages below ~2200 m directly date the onset of renewed exhumation and the formation of the Queen Valley pull-apart structure at 3.0 ± 0.5 Ma (Fig. 16). Because the samples were not collected along vertical transects, they are not suitable for estimation of paleogeothermal gradients. Further detailed work is needed to provide a more precise estimate for Pliocene geothermal gradients. On the basis of offset Pliocene volcanic units (e.g., Taylor, 1963) and the thickness of the Queen Valley basin fill, the total normal displacement along the Queen Valley Fault can be estimated at between ~2.5 and ~1.5 km. South of Marble Canyon, no samples yield (U-Th)/He ages younger than ca. 12 Ma, suggesting that Pliocene normal displacement decreases southward along the range front away from the Queen Valley pull-apart structure.

Apatite Fission-Track Modeling

Apatite fission-track data were modeled by using Monte Trax by Gallagher (1995) in order to more fully define the Cenozoic thermal evolution of the White Mountains. Partially annealed apatite fission-track apparent age and length data were used to constrain the thermal ($T < \sim 120$ °C) evolution of individual samples from the northern White Mountains (Fig. 17). Structurally shallow samples reveal an episode of Late Cretaceous–early Tertiary cooling, whereas the structurally deepest samples reveal detailed information about the late Miocene and Pliocene exhumation. Modeling results from a wide range of structural levels allow the complete reconstruction of the thermal history of the White Mountains crustal block since the Late Cretaceous–early Tertiary. Model runs of structurally shallow levels from the northern White Mountains suggest relatively rapid cooling in the Late Cretaceous–early Tertiary (~8 °C/m.y.) followed by protracted slow cooling through middle Miocene time at rates of ~1 °C/m.y. (Fig. 17). The cause of accelerated cooling in the early Tertiary is difficult to assess, but may be related to postmagmatic cooling, Laramide cooling/denudation, or possibly lithospheric refrigeration resulting from shallow-slab subduction (Dumitru et al., 1991). Subsequent cooling suggests slow erosional unroofing of the White Mountains as part of the inactive Sierra Nevada magmatic arc, prior to rapid cooling and exhumation of the White Mountains in the middle Miocene (Fig. 17).

Modeling results of partially annealed apatite fission-track samples from the northernmost White Mountains in the footwall of the Queen Valley Fault suggest that rapid middle Miocene cooling was followed by renewed cooling in the Pliocene between ca. 4 and 2 Ma. These results are in good agreement with (U-Th)/He age data that are indicative of renewed exhumation and formation of the Queen Valley pull-apart structure at ca. 3 Ma (Fig. 16).

THERMAL EVOLUTION OF THE WHITE MOUNTAINS BLOCK

The central part of the western Basin and Range province is characterized by contemporary high heat flow (~90 mW/m^2) (Saltus, 1991) and elevated geothermal gradients (~35 °C/km), as would be expected in a region of crustal attenuation resulting from lithospheric thinning and associated advective heating (e.g., Sass et al., 1976). These high heat-flow values are in sharp contrast to very low heat-flow values across much of the adjacent central Sierra Nevada (25–45 mW/m^2) (Henyey and Lee, 1976; Saltus and Lachenbruch, 1991). The anomalously low heat flow within the site of the former Mesozoic magmatic arc has been attributed to Late Cretaceous to early Tertiary shallow-slab subduction (Bird, 1988) resulting in refrigeration of the Sierran crust (Dumitru et al., 1991). Apatite fission-track work by Dumitru (1988, 1990) also suggests that low thermal gradients (5–15 °C/km) probably prevailed throughout the Cenozoic in the central Sierra Nevada. At lat 37–38°N, the boundary between high Basin and Range and low Sierran heat flow is rather sharp and is locally characterized by anomalously high heat flow (up to 150 mW/m^2) due to active volcanism (Long Valley and Inyo-Mono craters) (Saltus, 1991).

Thermochronological data in combination with structural reconstruction of the White Mountains can be used to constrain the Miocene preextensional thermal structure within the crust that is now part of the White Mountains fault block. Apatite fission-track and (U-Th)/He age constraints provide several avenues for setting limits on the geothermal gradient immediately prior to the onset of middle Miocene extension. If a Miocene mean annual surface temperature of 10 ± 5 °C is assumed, the distance from the Miocene paleosurface in the northern White Mountains to the base of the fission-track PAZ (~120 °C) or the (U-Th)/He PRZ (~85 °C) yields an estimate for the preextensional Miocene geothermal gradient of 15 ± 2 °C/km and 16 ± 2 °C, respectively, prior to the onset of extensional faulting at ca. 12 Ma (Fig. 13). The difference in depths between the base of the PAZ and the PRZ yields an estimate of ~15 °C/km.

TIMING OF TRANSTENSIONAL FAULTING IN THE WHITE MOUNTAINS AREA

The late Cenozoic to modern White Mountains are structurally bounded along the east-

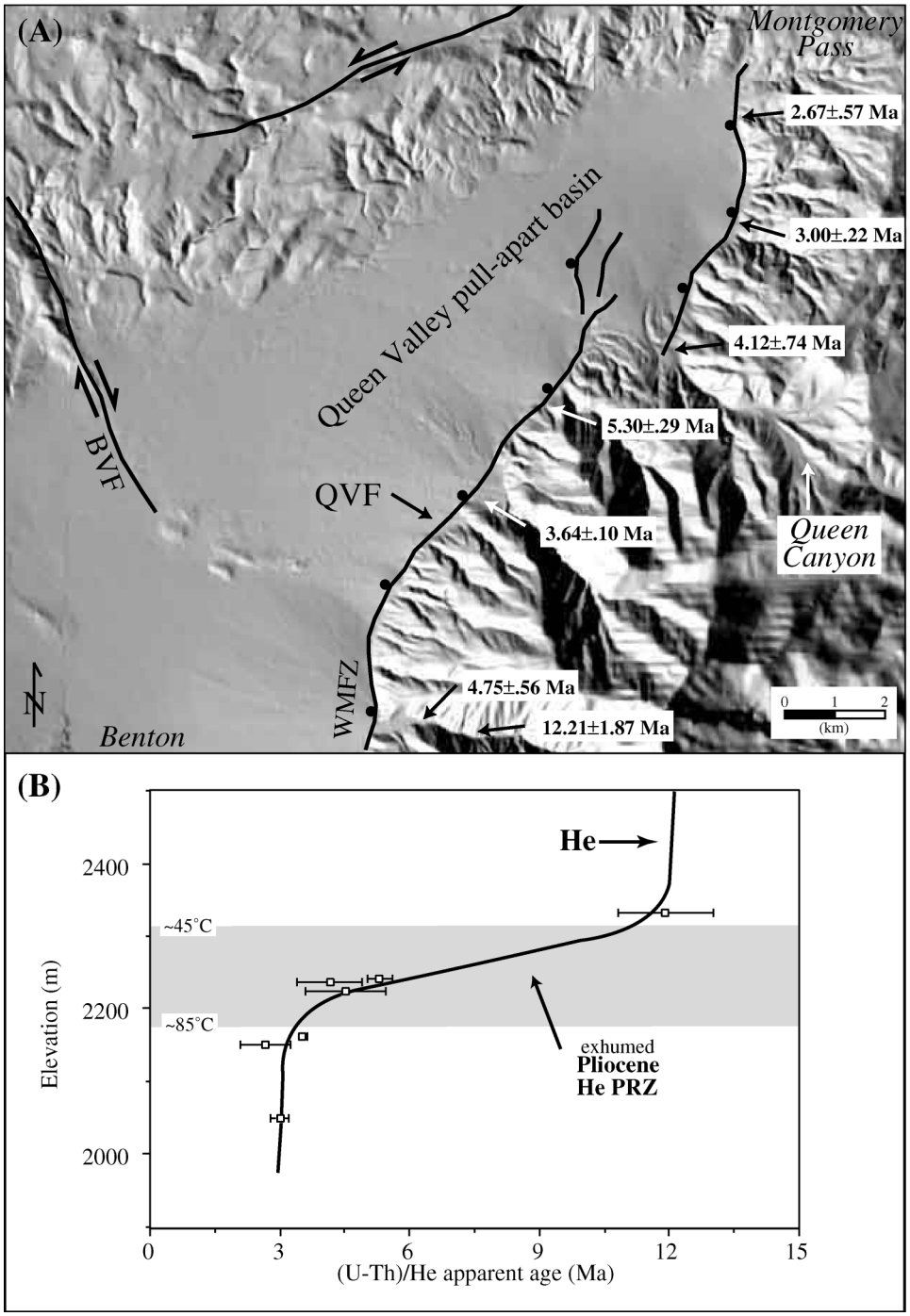

Figure 16. The northern White Mountains are truncated by the Pliocene Queen Valley Fault (QVF) bounding the northeast-trending Pliocene Queen Valley pull-apart basin. The Queen Valley Fault acts as a releasing bend, transferring displacement from the northern Owens Valley fault zone to the central Walker Lane belt. BVF—Benton Valley Fault. (A) Digital shaded-relief map of the northernmost White Mountains and Queen Valley showing Cenozoic faults and (U-Th)/He data from the footwall of the Queen Valley Fault. The Queen Valley Fault consists of two main fault strands in an en echelon geometry with dominant normal displacement consistent with northwest-southeast extension. (B) (U-Th)/He data from samples in the footwall of the Queen Valley pull-apart basin, showing a typical apparent age vs. elevation behavior; the inflection point at ~2200 m directly dates the onset of northwest-southeast transtension at ca. 3 Ma.

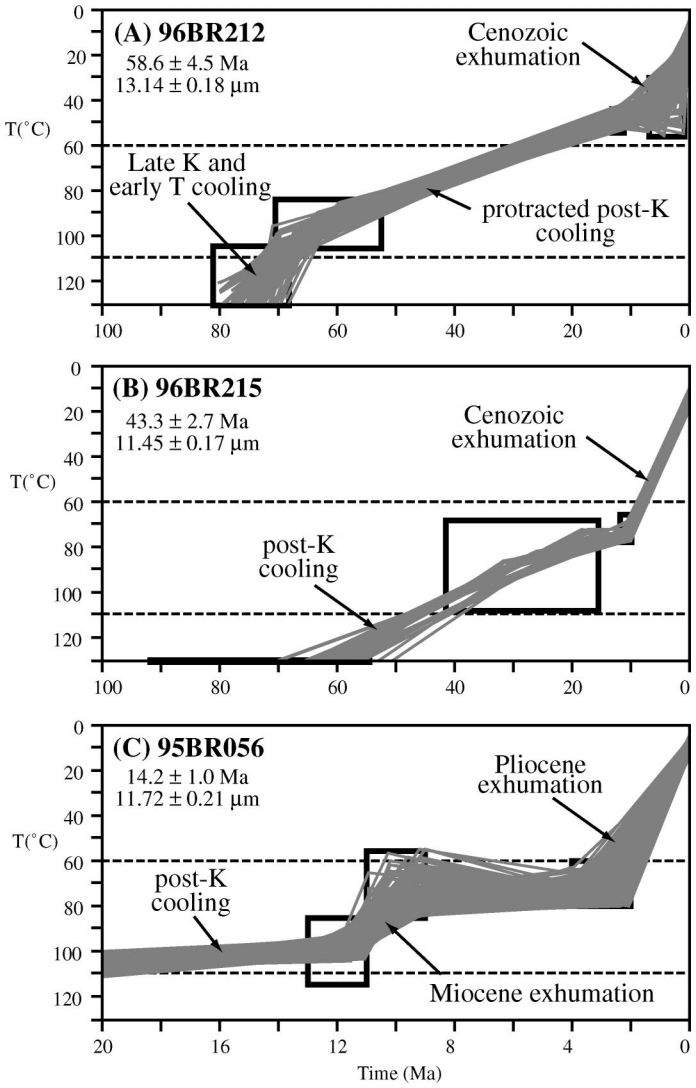

Figure 17. Apatite fission-track modeling results of representative samples from different structural levels of the northern White Mountains tilted footwall block and from the footwall of the Queen Valley Fault at the northern end of the White Mountains. (A) Model results of a sample from structurally shallow levels of the White Mountains fault block illustrate the Late Cretaceous and early Tertiary cooling history that is characterized by relatively fast cooling before ca. 60 Ma (~8 °C/m.y) and slow protracted post-Cretaceous cooling (~1 °C/m.y.) and erosional exhumation, followed by rapid cooling in the Cenozoic owing to extensional faulting along the White Mountains fault zone. (B) Model results of a sample from within the Miocene PAZ display the protracted post-Cretaceous cooling history (~1 °C/m.y.) and the rapid middle Miocene exhumation of the White Mountains footwall block. The results suggest that the sample's temperature prior to the onset of extension was ~70–80 °C, which is in good agreement with thermal reconstruction based on the apparent age vs. paleodepth diagram shown in Figure 14. (C) Model results for sample in the footwall of the Queen Valley Fault illustrate that the sample resided near the base of the Miocene PAZ and within the Pliocene PAZ in the footwall of the late Cenozoic Queen Valley pull-apart structure. The modeled thermal history clearly demonstrates a two-stage cooling and exhumation history consistent with Miocene extensional faulting between ca. 12 and 9 Ma and renewed Pliocene faulting starting at ca. 3 Ma.

ern and western flank by active right-lateral strike-slip fault systems—i.e., the Fish Lake Valley–Furnace Creek fault zone and the northern Owens Valley fault zone. The range is truncated at its southern and northern ends by northwest-dipping normal faults and pull-apart basins (Fig. 2).

The magnitude of right-lateral displacement on the Owens Valley fault zone is only poorly known (Stewart, 1988). The continuity of pre-Cenozoic batholithic rocks across Owens Valley suggests that only a small amount of right-lateral offset has been accommodated along the seismically active Owens Valley fault zone (Stewart, 1988). The displacement field along the fault zone is characterized by dip-slip motion along normal faults forming the eastern escarpment of the Sierra Nevada and strike-slip displacement along the main strand of the fault zone and represents a modern example of active strain partitioning. Several studies (Stewart, 1988; Reheis and Dixon, 1996) have proposed that the total right-lateral displacement along the Owens Valley fault zone decreases toward the north owing to the transfer of dextral slip to the east along right-stepping, northwest-striking faults. Queen Valley and Deep Springs Valley appear to represent pull-apart basins related to such right steps (Figs. 18 and 19), transferring slip from the Owens Valley fault zone to the Fish Lake Valley fault zone and the central part of the Walker Lane belt (Oldow, 1992; Reheis and Dixon, 1996; Lee et al., 2001). Queen Valley Fault is thought to form the northern termination of the Owens Valley fault zone, transferring most of the remaining displacement from the northern Owens Valley fault zone through the Coaldale fault system around the Mina deflection into the southern central Walker Lane belt. The (U-Th)/He thermochronological data from the footwall of the Queen Valley Fault indicate that exhumation associated with the opening of the Queen Valley pull-apart basin occurred at ca. 3 Ma (Fig. 18 and 19). The age of the Queen Valley pull-apart structure that forms the northern termination of the Owens Valley fault zone therefore is likely to reflect the onset of right-lateral strike-slip faulting in Owens Valley at ca. 3 Ma.

The right-lateral displacement along the Fish Lake Valley fault zone appears to die out in the Indian Creek–Chiatovich area of the northern White Mountains (Figs. 9 and 19) as a result of a right-step forming a pull-apart structure at the northern end of Fish Lake Valley (Figs. 2 and 18). The pull-apart basin is bounded by the Emigrant Peak fault zone, which transfers displacement from the Fish Lake Valley fault zone to the southern part of

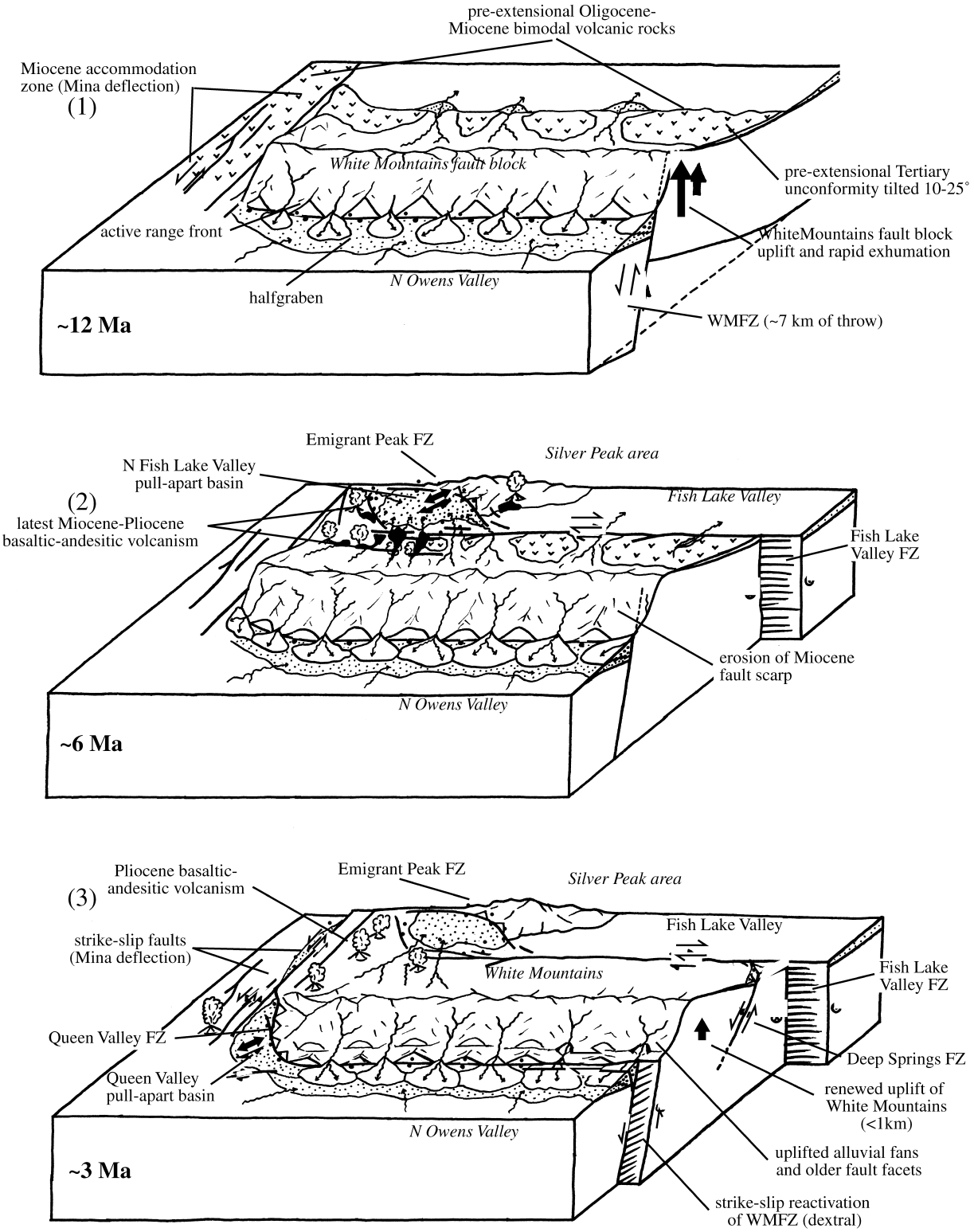

Figure 18. Summary block diagrams illustrating the tectonic evolution of the White Mountains area. (1) Middle Miocene east-west extension resulting in eastward tilting and uplift of the White Mountains crustal fault block. (2) Inception of strike-slip faulting at ca. 6 Ma in the Fish Lake Valley area and formation of a pull-apart basin at the northern termination of the Fish Lake Valley fault zone. (3) Right-lateral strike-slip reactivation of the White Mountains fault zone (WMFZ) and formation of pull-apart structures at the northern and southern end of the White Mountains, in Deep Springs Valley and Queen Valley. See text for more detailed discussion.

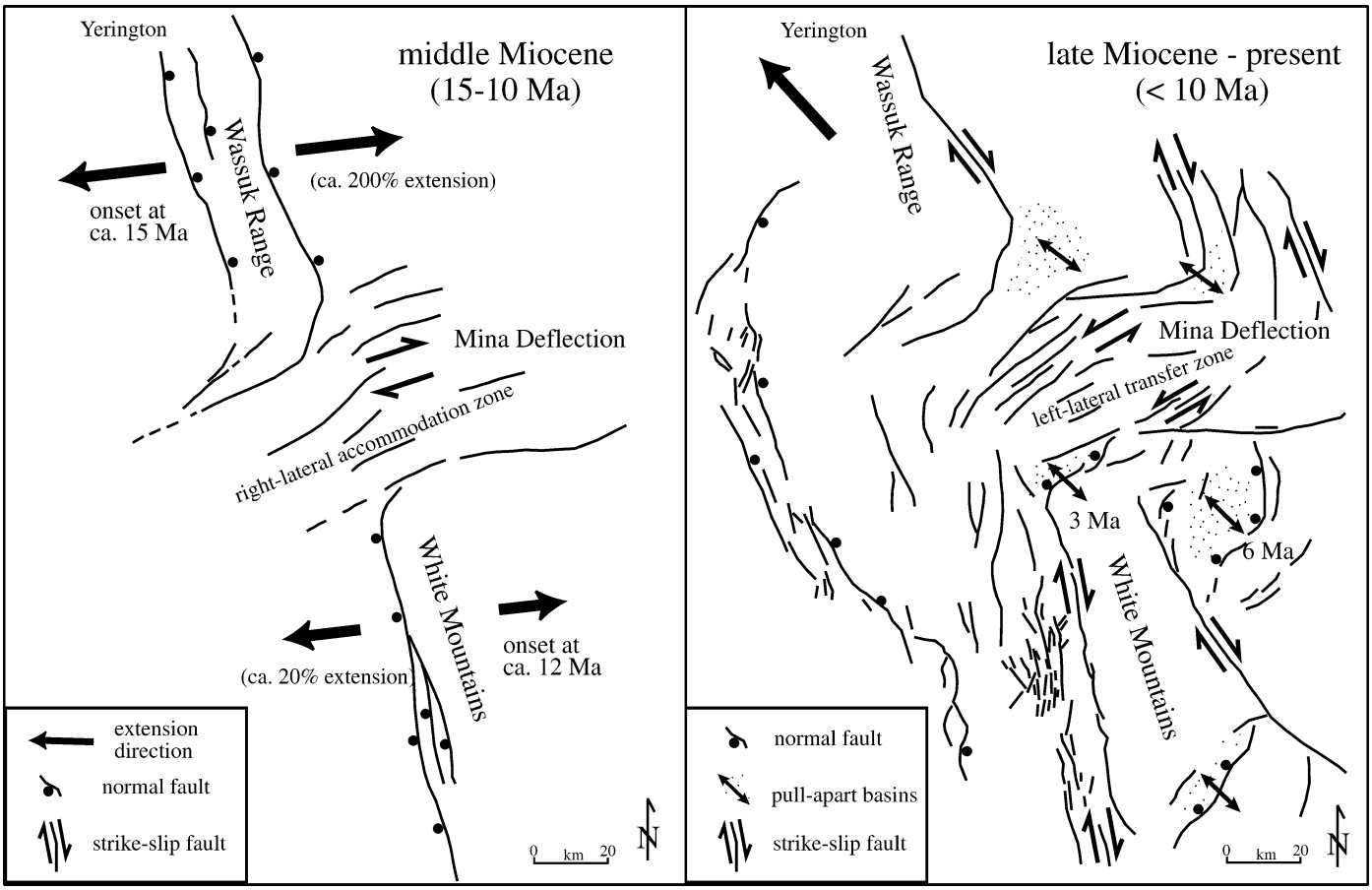

Figure 19. Schematic regional tectonic summary diagram illustrating the pronounced change in tectonic style and extension direction in the latest Miocene and Pliocene. The middle Miocene was characterized by dominant east-west (approximately) extension and normal faulting in the Wassuk-Yerington and White Mountains areas (Stockli et al., 2002; this study). The Mina deflection is proposed to have acted as an accommodation zone between the two extensional domains of opposite polarity. Beginning at ca. 10–6 Ma, the central-western Basin and Range started to undergo transtensional deformation as a result of northwest-southeast extension. This resulted in predominantly right-lateral transcurrent and transtensional deformation characterized by the formation of pull-apart structures in right-stepping transfer zones (e.g., Queen Valley and Silver Peak areas). Faulting appears to have migrated eastward in Pliocene time, as suggested by the inception of faulting in northern Fish Lake Valley (ca. 6 Ma) and northern Owens Valley (ca. 3 Ma). Cenozoic faults modified after Stewart (1988), Oldow (1992), and Reheis and Sawyer (1997).

the central Walker Lane belt (Reheis and Sawyer, 1997). The pull-apart system at the northern end of the Fish Lake Valley fault zone appears to have a relatively complex and long-lived history. Oldow (1992) described northwest-directed detachment faulting in the Silver Peak–Lone Mountain area to the east of northern Fish Lake Valley as representing a right-stepping, large-magnitude, extensional pull-apart system, transferring up to ~30–40 km of slip from the Fish Lake Valley fault zone to the central Walker Lane belt between 11 and 6 Ma. The Mineral Ridge detachment fault is cut by the high-angle Emigrant Peak fault zone and bracketed by ca. 6 Ma volcanism in the Silver Peak region (Fig. 18). Reheis and Sawyer (1997) demonstrated that faulting along the Emigrant Peak fault zone and formation of the Northern Fish Lake Valley pull-apart basin started at ca. 6–4 Ma. Activity along north-striking normal faults in the Indian Creek and Chiatovich Creek area related to the opening of the Northern Fish Lake Valley pull-apart basin is tightly dated by synextensional volcanism and suggests that faulting started at ca. 5.5 Ma (Fig. 18). The inception of strike-slip faulting along the Fish Lake Valley fault zone and Emigrant Peak fault zone and the formation of a pull-apart basin at the northern end of Fish Lake Valley occurred at ca. 6 Ma.

DISCUSSION

This study presents new structural, stratigraphic, and geochronological data that conclusively demonstrate a two-stage Cenozoic tectonic and thermal evolution of the White Mountains region (Fig. 18). The White Mountains fault block represents a crustal block tilted 25° to the east that underwent rapid exhumation due to extensional faulting along the White Mountains fault zone starting at ca. 12 Ma (Fig. 18). The structural reconstruction of the footwall block indicates that the fault zone accommodated up to 8 km of dip-slip displacement as a consequence of middle Miocene east-west extension. The thermochronological data suggest that samples from the base of the White Mountains footwall cooled rapidly from >120 °C to <40 °C in the middle Miocene, indicating that the White Mountains were rapidly exhumed at 12 Ma. This finding contradicts the suggestion of Lued-

decke et al. (1998) that uplifted alluvial deposits along the western range front, dated at ca. 3.5–2.1 Ma, represent evidence that initial exhumation of the White Mountains did not start until ca. 3 Ma. In our opinion these uplifted Pliocene alluvial piedmont surfaces record renewed Pliocene exhumation of <1 km and imply that the southern White Mountains were indeed already elevated to near their present topographic relief by that time.

The onset of rapid middle Miocene exhumation and extensional faulting in the White Mountains is slightly younger than major extension in the central part of the northern Basin and Range province (ca. 18–15 Ma; Stockli, 1999; Stockli et al., 2002), but is distinctly older than faulting along the eastern Sierra Nevada (Huber, 1981; Unruh, 1991; Surpless et al., 2002). In the Yerington district to the north of the Mina deflection (Fig. 19), large-magnitude Miocene extension in the Singatse Range and Wassuk Range began at 15 Ma and was accommodated by east-dipping normal faults (Proffett, 1977; Dilles and Gans, 1995; Surpless et al., 2002; Stockli et al., 2002). Extensional faulting on east-dipping faults in the Yerington area appears to have been roughly coeval with motion on the west-dipping White Mountains fault zone, implying that east-striking faults of the Mina deflection acted as an antithetic accommodation zone linking two middle Miocene extensional domains with opposite fault polarities (Fig. 19) (Axen, 1995; Stewart, 1998). Such a scenario demands substantial right-lateral motion on currently left-lateral east-trending faults within the Mina deflection in middle Miocene time. Stewart (1985) reported that these east-trending faults were indeed characterized by earlier right-lateral displacement, lending further support to the hypothesis that the Mina deflection acted as a Miocene accommodation zone.

After ca. 6 Ma the White Mountains area was characterized by predominantly transcurrent and transtensional deformation accommodating northwest-southeast extension (Figs. 18 and 19). Fault-controlled andesitic and rhyolitic volcanism in the northern Fish Lake Valley area on the eastern side of the White Mountains beginning at ca. 6 Ma signals the onset of transtensional faulting along the Fish Lake Valley fault zone and the formation of a pull-apart structure transferring right-lateral slip from that fault zone to the central Walker Lane belt. Starting at ca. 3 Ma, right-lateral shearing affected the western flank of the White Mountains along part of the Owens Valley fault zone (Fig. 18). Fault kinematic and thermochronological data from the western range front of the White Mountains illustrate the Pliocene reactivation of the White Mountains fault zone as a normal-oblique right-lateral fault system with dominant strike-slip displacement. Geomorphologic and seismotectonic information corroborate the reactivation of the White Mountains fault zone as a right-lateral fault system (DePolo, 1989). The normal-slip component resulted in moderate renewed exhumation of the White Mountains beginning at ca. 3 Ma (Fig. 18). This renewed phase of faulting and exhumation has been well documented by previous studies (DePolo, 1989; Lueddecke et al., 1998).

At its northern and southern ends, the White Mountains fault block is bounded by Pliocene pull-apart structures bounded by northwest-dipping normal-fault zones (Figs. 18 and 19). The Deep Springs Fault in the south and the Queen Valley Fault in the north are right-stepping fault zones that transfer displacement from the Owens Valley fault zone to the Fish Lake Valley fault zone–Furnace Creek fault zone and eventually to the central Walker Lane belt (Fig. 19). The Queen Valley pull-apart basin is situated at the northern termination of the Owens Valley fault zone and appears to transfer most of the remaining right-lateral displacement from the Owens Valley fault via the Coaldale Fault into the southern-central Walker Lane belt (Fig. 19). The timing of inception of transtensional faulting and pull-apart basin formation at ca. 3 Ma in the Queen Valley area suggests that the inception of strike-slip faulting in northern Owens Valley and normal faulting along the eastern escarpment of the Sierra Nevada occurred at ca. 3 Ma as well. This interpretation is supported by the ages of sedimentary basin fill in the northern Owens Valley (ca. 4–2 Ma, Pinter and Keller, 1995) and in the southern Owens Valley (6–2.5 Ma, Bacon et al., 1979) and is in good agreement with the proposed Pliocene tilting of the Sierra Nevada (e.g., Huber, 1981; Unruh, 1991).

These constraints on the timing of onset of right-lateral shearing in the White Mountains area indicate that the locus of strike-slip deformation migrated westward in late Miocene and Pliocene time, beginning at ca. 11–6 Ma in the Silver Peak area, at ca. 6 Ma in Fish Lake Valley, and at ca. 3 Ma in the Owens Valley area (Fig. 18). As a consequence of the westward migration of transcurrent faulting from the Fish Lake Valley area to the Owens Valley fault zone, fault activity along the easternmost faults appears to have diminished. Oldow (1992) suggested that such westward migration might eventually result in abandonment of part of the Mina deflection and the central Walker Lane belt and northward migration of strike-slip displacement.

This study demonstrates that Miocene extensional faulting and Pliocene transcurrent deformation in the White Mountains are not the result of strain partitioning, but represent two temporally distinct tectonic episodes (Figs. 18 and 19). Extensional faulting and exhumation of the White Mountains fault block was initiated at ca. 12 Ma as the result of east-west extension, only slightly later than extension in large parts of the central Basin and Range province in the middle Miocene (Stockli, 1999; Stockli et al., 2002). Pliocene transcurrent shearing resulted in the progressive reactivation of extensional structures and truncation of the east-tilted Miocene White Mountains footwall block by transtensional pull-apart structures in Deep Springs and Queen Valley (Fig. 19).

ACKNOWLEDGMENTS

This project was made possible through financial support by Stanford University McGee and Shell fund grants, a University of California White Mountains Research Station fellowship (to Stockli), and National Science Foundation grants EAR-9417937 and EAR-9725371 (to E. Miller and Dumitru). Stockli thanks L. Stockli, J. Hourigan, B. Surpless, and the staff of the White Mountains Research Station for assistance in the field; L. Hedges and D. Miller for laboratory assistance, and F. Orr for aerial support. We also thank C. DePolo, W.G. Ernst, B. Wernicke, M. House, and S. Klemperer for insightful and inspiring discussions and P. Fitzgerald, R. Scott, and D. Foster for improving the final version of the manuscript.

REFERENCES CITED

Axen, G.J., 1995, Extensional segmentation of the main Gulf escarpment, Mexico and United States: Geology, v. 23, p. 515–518.

Bacon, C.R., Ciovannetti, D.M., Duffield, W.A., Dalrymple, G.B., and Drake, R.E., 1979, Age of the Coso Formation, Inyo County, California: U.S. Geological Survey Bulletin 1527,18 p.

Bird, P., 1988, Formation of the Rocky Mountains, western United States: A continuum computer model: Science, v. 239, p. 1501–1507.

Bryant, W.A., 1984, Evidence of recent faulting along the Owens Valley, Round Valley, and White Mountains fault zones, Inyo and Mono Counties: California Division of Mines and Geology, OFR84–54SAC,4 p.

Cockerham, R.S., and Corbett, E.J., 1987, The July 1986 Chalfant Valley, California, earthquake sequence: Preliminary results: Geological Society of America Bulletin, v. 77, p. 280–289.

Corrigan, J.D., 1991, Inversion of apatite fission track data for thermal history information: Journal of Geophysical Research, v. 96, p. 10,347–10,360.

Crowley, K.D., Cameron, M., and Schaefer, R.L., 1991, Experimental studies of annealing of etched fission tracks in fluorapatite: Geochimica et Cosmochimica Acta, v. 55, p. 1449–1465.

Crowder, D.F., and Ross, D.C., 1972, Permian (?) to Jurassic (?) metavolcanic and related rocks that mark a major structural break in the northern White Mountains:

U.S. Geological Survey Professional Paper 800-B, p. B195–B203.

Crowder, D.F., Robinson, P.T., and Harris, D.L., 1972, Geologic map of the Benton Quadrangle, Mono County, California and Esmeralda and Mineral Counties, Nevada: U.S. Geological Survey Geologic Quadrangle Map GQ-1012, 1:62,500.

Crowder, D.F., McKee, E.H., Ross, D.C., and Krauskopf, K.B., 1973, Granitic rocks of the White Mountains area, California–Nevada: Age and regional significance: Geological Society of America Bulletin, v. 84, p. 285–296.

DePolo, C.M., 1989, Seismotectonics of the White Mountains fault system, east-central California and west-central Nevada [M.S. thesis]: Reno, University of Nevada, 354 p.

DePolo, C.M., and Ramelli, A.R., 1987, Preliminary report on surface fractures along the White Mountains fault zone associated with the July 1986 Chalfant Valley earthquake sequence: Seismological Society of America Bulletin, v. 77, p. 290–296.

DePolo, C.M., Peppin, W.A., and Johnson, P.A., 1993, Contemporary Tectonics, seismicity, and potential earthquake sources in the White Mountains seismic gap, west-central Nevada and east-central California, USA: Tectonophysics, v. 22, p. 271–299.

Dilles, J., and Gans, P.B., 1995, The chronology of Cenozoic volcanism and deformation in the Yerington area, western Basin and Range and Walker Lane: Geological Society of America Bulletin, v. 107, p. 474–486.

Dixon, T.H., Robaudo, S., Lee, J., and Reheis, M.C., 1995, Constraints on present-day Basin and Range deformation from space geodesy: Tectonics, v. 14, p. 755–772.

Dixon, T.H., Miller, M., Farina, F., Wang, H., and Johnson, D., 2000, Present-day motion of the Sierra Nevada block and some tectonic implications for the Basin and Range province, North American Cordillera: Tectonics, v. 19, p. 1–24.

Dumitru, T.A., 1988, Subnormal geothermal gradients in the Great Valley forearc basin, California, during Franciscan subduction: A fission track study: Tectonics, v. 7, p. 1201–1221.

Dumitru, T.A., 1993, A new computer-automated microscope stage system for fission track analysis: Nuclear Tracks and Radiation Measurements, v. 21, p. 575–580.

Dumitru, T.A., 1990, Subnormal Cenozoic geothermal gradients in the extinct Sierra Nevada magmatic arc: Consequences of Laramide and post-Laramide shallow-angle subduction: Journal of Geophysical Research, v. 95, p. 4925–4941.

Dumitru, T.A., 2000, Fission-track geochronology in Quaternary geology, *in* Noller, J.S., Sowers, J.M., and Lettis, W.R., eds., Quaternary geochronology: Methods and applications: American Geophysical Union Reference Shelf, v. 4, p. 131–156.

Dumitru, T.A., Gans, P.B., Foster, D.A., and Miller, E.L., 1991, Refrigeration of the western Cordilleran lithosphere during Laramide shallow-angle subduction: Geology, v. 19, p. 1145–1148.

Dunne, G.C., 1986, Mesozoic evolution of the southern Inyo Range, Darwin Plateau, and Argus and Slate Ranges, east-central California, *in* Dunne, G.C., ed., Mesozoic and Cenozoic structural evolution of selected areas, east-central California: Los Angeles, Geological Society of America Annual Cordilleran Section Meeting, Guidebook and Volume, Field Trips 2 and 14, p. 3–43.

Dunne, G.C., Gulliver, R.M., and Sylvester, A.G., 1978, Mesozoic evolution of the White, Inyo, Argus, and Slate Ranges, eastern California, *in* Howell, D.G., and McDougall, K.A., eds., Mesozoic paleogeography of the western United States: Society of Economic Paleontologists and Mineralogists, Pacific Coast Paleogeography Symposium, p. 189–207.

Ernst, W.G., 1987, Geology of the Mount Barcroft–Blanco Mountain area, eastern California: Geological Society of America Map and Chart Series, MCH066, scale 1: 24,000. 1 sheet.

Farley, K.A., Wolf, R.A., and Silver, L.T., 1996, The effects of long alpha-stopping distances on (U-Th)/He ages: Geochimica et Cosmochimica Acta, v. 60, p. 4223–4229.

Farley, K.A., 2002, (U-Th)/He dating: Techniques, calibrations, and applications, *in* Porcelli, D., Ballentine, C.J., and Wieler, R., eds., Noble gases in geochemistry and cosmochemistry: Mineralogical Society of America Mineralogical Society of America Reviews of Mineralogy, v. 47, p. 819–844.

Farley, K.A., and Stockli, D.F., 2002, (U-Th)/He dating of phosphates: Apatite, monazite, and xenotime, *in* Kohn, M., Rakovan, J., and Hughes, J.M., eds., Phosphates: Mineralogical Society of America Reviews of Mineralogy, v. 47, p. 559–578.

Fitzgerald, P.G., 1992, The Transantarctic Mountains in southern Victoria Land: The application of apatite fission track analysis to a rift-shoulder uplift: Tectonics, 11, p. 634–662.

Fitzgerald, P.G., 1994, Thermochronologic constraints on post-Paleozoic tectonic evolution of the central Transantarctic Mountains, Antarctica: Tectonics, v. 13, p. 818–836.

Fitzgerald, P.G., and Gleadow, A.J.W., 1990, New approaches in fission track geochronology as a tectonic tool: Examples from the Transantarctic Mountains: Nuclear Tracks and Radiation Measurements, v. 17, p. 351–357.

Fitzgerald, P.G., Fryxell, J.E., and Wernicke, B.P., 1991, Miocene crustal extension and uplift in southeastern Nevada: Constraints from fission track analysis: Geology, v. 19, p. 1013–1016.

Fleischer, R.L., Price, P.B., and Walker, R.M., 1975, Nuclear tracks in solids: Berkeley, California, University of California Press, 605 p.

Foster, D.A., Miller, D.S., and Miller, C.F., 1991, Tertiary extension in the Old Woman Mountains area, California: Evidence from apatite fission track analysis: Tectonics, v. 10, p. 875–886.

Foster, D.A., Gleadow, A.J.W., Reynolds, S.J., and Fitzgerald, P.G., 1993, The denudation of metamorphic core complexes and the reconstruction of the Transition zone, west-central Arizona: Constraints from apatite fission-track thermochronology: Journal of Geophysical Research, v. 98, p. 2167–2185.

Foster, D.A., and Gleadow, A.J.W., 1996, Structural framework and denudation history of the flanks of the Kenya and Anza Rifts, east Africa: Tectonics, v. 15, p. 258–271.

Galbraith, R.F., 1981, On statistical models for mixed fission track ages: Nuclear Tracks and Radiation Measurements, v. 13, p. 471–478.

Galbraith, R.F., and Laslett, G.M., 1983, Statistical models for mixed fission track ages: Nuclear Tracks and Radiation Measurements, v. 21, p. 459–470.

Green, P.F., 1981, A new look at statistics in fission track dating: Nuclear Tracks and Radiation Measurements, v. 5, p. 77–86.

Gallagher, K., 1995, Evolving temperature histories from apatite fission-track data: Earth and Planetary Science Letters, v. 136, p. 421–43.

Gans, P.B., Miller, E.L., Brown, R., Houseman, G., and Lister, G.S., 1991, Assessing the amount, rate and timing of tilting in normal fault blocks: A case study of tilted granites in the Kern–Deep Creek Mountains, Utah: Geological Society of America Abstracts with Programs, v. 23, no. 7, p. 28.

Gleadow, A.J.W., Duddy, I.R., Green, P.F., and Hegarty, K.A., 1986a, Fission track lengths in the apatite annealing zone and the interpretation of mixed ages: Earth and Planetary Science Letters, v. 78, p. 245–254.

Gleadow, A.J.W., Duddy, I.R., Green, P.F., and Lovering, J.F., 1986b, Confined fission track lengths in apatite: A diagnostic tool for thermal history analysis: Contributions to Mineralogy and Petrology, v. 94, p. 405–415.

Gleadow, G.W., belton, D.X., Kohn, B.P., and Brown, R.W., 2002, Fission track dating of phosphate minerals and the thermochronology of apatite, *in* Kohn, M., Rakovan, J., and Hughes, J.M., eds., Phosphates: Mineralogical Society of America Mineralogical Society of America Reviews of Mineralogy, v. 48, p. 579–611.

Green, P.F., Duddy, I.R., Gleadow, A.J.W., and Lovering, J.F., 1989a, Apatite fission-track analysis as a paleotemperature indicator for hydrocarbon exploration, *in* Naeser, N.D., and McCullogh, T.H., eds., Thermal history of sedimentary basins: Methods and case histories: New York, Springer-Verlag, p. 181–195.

Green, P.F., Duddy, I.R., Laslett, G.M., Hegarty, K.A., Gleadow, A.J.W., and Lovering, J.F., 1989b, Thermal annealing of fission tracks in apatite: 4. Quantitative modeling techniques and extension to geological timescales: Chemical Geology, v. 79, p. 155–182.

Hanson, R.B., 1986, Geology of Mesozoic metavolcanic and metasedimentary rocks, northern White Mountains, California [Ph.D. thesis]: Los Angeles, University of California, 295 p.

Hanson, R.B., 1987, Superimposed deformations in the development of a shear zone: An example from the northern White Mountains, California: Geological Society of America Abstracts with Programs, v. 19, no. 7, p. 693.

Hanson, R.B., 1997, A tale of 10 plutons, revisited: Age of granitic rocks in the White Mountains, California and Nevada: Discussion and reply: Geological Society of America Bulletin, v. 109, p. 1631–1632.

Hanson, R.B., Saleeby, J.B., and Fates, D.G., 1987, Age and tectonic setting of Mesozoic metavolcanic and metasedimentary rocks, northern White Mountains, California: Geology, v. 15, p. 1074–1078.

Hardyman, R.F., and Oldow, J.S., 1991, Tertiary tectonic framework and Cenozoic history of the central Walker Lane, Nevada, *in* Raines, G.L., Lisle, R.E., Schafer, R.W., and Wilkinson, W.H., eds., Geology and ore deposits of the Great Basin, symposium proceedings: Reno, Nevada, Geological Society of Nevada, p.279–301.

Henyey, T.L., and Lee, C.F., 1976, Heat flow in Lake Tahoe, California-Nevada and the Sierra Nevada–Basin and Range transition: Geological Society of America Bulletin, v. 87, p. 1179–1187.

House, M.A., Farley, K.A., and Kohn, B.P., 1999, An empirical test of helium diffusion in apatite: Borehole data from the Otway Basin, Australia: Earth and Planetary Science Letters, v. 170, p. 463–474.

Howard, K.A., and Foster, D.A., 1996, Thermal and unroofing history of a thick, tilted Basin-and-Range crustal section in the Tortilla Mountains, Arizona: Journal of Geophysical Research, v. 101, p. 511–522.

Huber, N.K., 1981, Amount and timing of late Cenozoic uplift and tilt of the central Sierra Nevada, California—Evidence form the upper San Joaquin River basin: U.S. Geological Survey Professional Paper 1197, 28 p.

Hurford, A.J., and Green, P.F., 1983, The zeta calibration of fission track dating: Chemical Geology, v. 41, p. 285–317.

John, B.E., and Foster, D.A, 1993, Structural and thermal constraints on the initiation angle of detachment faulting in the southern Basin and Range: The Chemehuevi Mountains case study: Geological Society of America Bulletin, v. 105, p. 1091–1108.

John, B.E., and Howard, K.A., 1995, Rapid extension recorded by cooling-age patterns and brittle deformation, Naxos, Greece: Journal of Geophysical Research, v. 100, p. 9969–9979.

Kamp, P.J., 1997, Paleogeothermal gradient and deformation style, Pacific front of the Southern Alps orogen: Constraints from fission track thermochronology: Tectonophysics, v. 271, p. 37–58.

Krauskopf, K.B., 1968, A tale of 10 plutons: Geological Society of America Bulletin, v. 79, p. 1–17.

Krauskopf, K.B., 1971, Geologic map of the Mount Barcroft Quadrangle, California-Nevada: U.S. Geological Survey Geologic Quadrangle Map GQ-960, scale 1: 62,500.

Ketcham, R.A., Donelick, R.A., Donelick, M.B., 2002, AFTSolve: A program for multi-kinetic modeling of apatite fission-track data: Geological Materials Research, v. 2, no. 1.

Laslett, G.M., Kendall, W.S., Gleadow, A.J.W., and Duddy, I.R., 1982, Bias in the measurements of fission track length distributions: Nuclear Tracks and Radiation Measurements, v. 6, p. 79–85.

Laslett, G.M., Green, P.F., Duddy, I.R., and Gleadow,

A.J.W., 1987, Thermal annealing of fission tracks in apatite: 2. A quantitative analysis: Chemical Geology, v. 65, p. 1–13.

Lee, J., Rubin, C., and Calvert, A., 2001, Quaternary faulting history along the Deep Springs Fault, California: Tectonics, v. 113, p. 855–869.

Lienkaemper, J.J., Pezzopane, S.K., Clark, M.M., and Rymer, M.J., 1987, Fault fractures formed in association with the 1986 Chalfant Valley, California, earthquake sequence: Preliminary report: Seismological Society of America Bulletin, v. 77, p. 297–305.

Locke, A., Billingsley, P.R., and Mayo, E.B., 1940, Sierra Nevada tectonic pattern: Geological Society of America Bulletin, v. 51, p. 513–540.

Lueddecke, S.B., Pinter, N., and Gans, P.B., 1998, Plio–Pleistocene ash falls, sedimentation, and range-front faulting along the White-Inyo Mountains front, California: Journal of Geology, v. 106, p. 511–522.

McKee, E.H., Diggles, M.F., Donahoe, J.L., and Elliot, G.S., 1982, Geologic map of the White Mountains Wilderness and Roadless Areas, California, and Nevada: U.S. Geological Survey Miscellaneous Field Studies Map MF-1361-A, scale 1:62,500.

McKee, E.H., and Conrad, J.E., 1996, A tale of 10 plutons, revisited: Age of granitic rocks in the White Mountains, California and Nevada: Geological Society of America Bulletin, v. 108, p. 1515–1527.

Miller, E.L., Dumitru, T.A., Brown, R., and Gans, P.B., 1999, Rapid Miocene slip on the Snake Range–Deep Creek Range fault system, east-central Nevada: Geological Society of America Bulletin, v. 111, p. 886–905.

Miller, M.M., Johnson, D.J., Dixon, T.H., and Dokka, R.K., 2001, Refined kinematics of the eastern California shear zone from GPS observations, 1993–1994: Journal of Geophysical Research, v. 106, p. 2245–2263.

Naeser, C.W., 1979, Fission track dating and geological annealing of fission tracks, *in* Jaeger, E., and Hunziker, J.C., eds., Lectures in isotope geology: New York, Springer-Verlag, p. 154–169.

Naeser, C.W., 1981, The fading of fission tracks in the geologic environment—Data from deep drillholes [abs.]: Nuclear Tracks and Radiation Measurements, v. 5, p. 248–250.

Oldow, J.S., 1992, Late Cenozoic displacement partitioning in the northwestern Great Basin, *in* Craig, S.D., ed., Structure, tectonics and mineralization of the Walker Lane, Walker Lane symposium proceedings volume: Reno, Nevada, Geological Society of Nevada, p. 17–52.

Oldow, J.S., Kohler, G., and Donelick, R.A., 1994, Late Cenozoic extensional transfer in the Walker Lane strike-slip belt, Nevada: Geology, v. 22, p. 637–640.

Pakiser, L.C., Kane, M.F., and Jackson, W.H., 1964, Structural geology and volcanism of Owens Valley region, California: A geophysical study: U.S. Geological Survey Professional Paper 438, 68 p.

Pinter, N., and Keller, E.A., 1995, Geomorphological analysis of neotectonic deformation, northern Owens Valley, California: Geologische Rundschau, v. 84, p. 200–212.

Proffett, J.M., Jr., 1977, Cenozoic geology of the Yerington District, Nevada, and implications for the nature and origin of Basin and Range faulting: Geological Society of America Bulletin, v. 88, p. 247–266.

Reheis, M.C., Sawyer, T.L., Slate, J.L., and Gillespie, A.R., 1993, Geologic map of late Cenozoic deposits and faults in the southern part of the Davis Mountain 15′ quadrangle, Esmeralda County, Nevada: U.S. Geological Survey Miscellaneous Investigation Series Map I-2342, scale 1:24,000.

Reheis, M.C., and Dixon, T.H., 1996, Kinematics of the eastern California shear zone: Evidence for slip transfer from Owens and Saline Valley fault zones to Fish Lake Valley fault zone: Geology, v. 24, p. 339–342.

Reheis, M.C., and Sawyer, T.L., 1997, Late Cenozoic history and slip rates of the Fish Lake Valley, Emigrant Peak, and Deep Springs fault zones, Nevada and California: Geological Society of America Bulletin, v. 109, p. 280–299.

Reiners, P.W., Brady, R., Farley, F.A., Fryxell, J.E., Wernicke, B., and Lux, D., 2000, Helium and argon thermochronometry of the Gold Butte block, South Virgin Mountains, Nevada: Earth and Planetary Science Letters, v. 178, p. 315–326.

Reiners, P.W., 2002, (U-Th)/He chronometry experiences a renaissance: Eos (Transactions, American Geophysical Union), v. 83, p. 21–27.

Robinson, P.T., McKee, E.H., and Moiola, R., 1968, Cenozoic volcanism and sedimentation, Silver Peak region, western Nevada and adjacent California, *in* Studies in volcanology: Geological Society of America Memoir 116, p. 577–611.

Robinson, P.T., and Crowder, D.F., 1973, Geologic map of the Davis Mountain quadrangle, Esmeralda and Mineral Counties, Nevada and Mono County, California: U.S. Geological Survey Geologic Quadrangle Map GQ-1078, scale 1: 62,500.

Robinson, P.T., and Stewart, J.H., 1984, Uppermost Oligocene and lowermost Miocene ash-flow tuffs of western Nevada: U.S. Geological Survey Bulletin 1557, 53 p.

Rogers, A.M., Harmsen, S.C., Corbett, E.J., Priestly, K., and DePolo, D., 1991, The seismicity of Nevada and some adjacent parts of the Great Basin, *in* Slemmons, D.B., Engdahl, E.R., Zoback, M.D., and Blackwell, D.D., eds., Neotectonics of North America: Boulder, Colorado, Geological Society of America, Geology of North America, v. 1, p. 153–184.

Russell, B.J., 1977, A structural break and kinematics of faulting in the White Mountains, California: Geological Society of America Abstracts with Programs, v. 9, p. 491.

Sass, J.H., Diment, W.H., Lachenbruch, A.H., Marshall, B.V., Munroe, R.J., Moses, T.H., Jr., and Urban, T.C., 1976, A new heat-flow contour map of the conterminous United States: U.S. Geological Survey Open-File Report 76–0756, 24 p.

Saltus, R.W., 1991, Gravity and heat flow constraints on the Cenozoic tectonics of the western U.S. Cordillera [Ph.D. thesis]: Stanford, California, Stanford University, 241 p.

Saltus, R.W., and Lachenbruch, A.H., 1991, Thermal evolution of the Sierra Nevada: Tectonic implications of new heat flow data: Tectonics, v. 10, p. 325–344.

Savage, J.C., 1983, Strain accumulation in western United States: Annual Review of Earth and Planetary Sciences, v. 11, p. 11–43.

Speed, R., 1979, Extensional faulting in the Great Basin: Kinematics and possible changes with depth, *in* Speed, R., ed., Analysis of actual fault zones in bedrock: Proceedings and conference: U.S. Geological Survey Open-File Report 79–1239, p. 121–138.

Stevens, C.H., Stone, P., Dunne, G.C., Greene, D.C., Walker, J.D., and Swanson, B.J., 1997, Paleozoic and Mesozoic evolution of east-central California: International Geology Review, v. 39, p. 788–829.

Stewart, J.H., 1985, East-trending dextral faults in the western Great Basin: An explanation for anomalous trends of pre-Cenozoic strata and Cenozoic faults: Tectonics, v. 4, p. 547–564.

Stewart, J.H., 1988, Tectonics of the Walker Lane belt, western Great Basin: Mesozoic and Cenozoic deformation in a zone of shear, *in* Ernst, W.G., ed., Metamorphism and crustal evolution of the western United States (Rubey volume VII): Englewood Cliffs, New Jersey, Prentice-Hall, p. 683–713.

Stewart, J.H., 1992a, Paleogeography and tectonic setting of Miocene continental strata in the northern part of the Walker Lane belt, *in* Craig, S.D., ed., Structure, tectonics and mineralization of the Walker Lane: Walker Lane symposium proceedings volume: Reno, Nevada, Geological Society of Nevada, p. 53–61.

Stewart, J.H., 1992b, Walker Lane belt, Nevada and California: An overview, *in* Craig, S.D., ed., Structure, tectonics and mineralization of the Walker Lane: Walker Lane symposium proceedings volume: Reno, Nevada, Geological Society of Nevada, p. 1–16.

Stewart, J.H., 1998, Regional characteristics, tilt domains, and extensional history of the later Cenozoic Basin and Range province, western North America: Geological Society of America Special Paper 323 p. 47–74.

Stewart, J.H., and Carlson, J.E., 1976, Geologic map of Nevada: U.S. Geological Survey, scale 1:500,000.

Stockli, D.F., 1999, Regional timing and spatial distribution of Miocene extension in the northern Basin and Range province [Ph.D. thesis]: Stanford, California, Stanford University, 239 p.

Stockli, D.F., Farley, K.A., and Dumitru, T.A., 2000, Calibration of the apatite (U-Th)/He thermochronometer on an exhumed fault block, White Mountains, California: Geology, v. 28, p. 983–986.

Stockli, D.F., Linn, J.K., Walker, J.D., and Dumitru, T.A., 2001, Miocene unroofing of the Canyon Range during extension along the Sevier Desert detachment, west-central Utah: Tectonics, v. 20, p. 289–307.

Stockli, D.F., Surpless, B.E., Dumitru, T.A., and Farley, K.A., 2002, Thermochronological constraints on the timing and magnitude of Miocene and Pliocene extension in the central Wassuk Range, western Nevada: Tectonics, v. 21, no. 4, 10.1029/2001TC001295.

Surpless, B.E., Stockli, D.F., Dumitru, T.A., and Miller, E.L., 2002, Two phase westward encroachment of Basin and Range extension into the northern Sierra Nevada: Tectonics, v. 21, no. 1, 10.1029/2000TC001257.

Taylor, R.L., 1963, Cenozoic volcanism, block faulting, and erosion in the northern White Mountains, Nevada [M.S. thesis]: Berkeley, University of California, 95 p.

Unruh, J.R., 1991, The uplift of the Sierra Nevada and implications for late Cenozoic epeirogeny in the western Cordillera: Geological Society of America Bulletin, v. 103, p. 1395–1404.

Weiss, S.I., Noble, D.C., Worthington, J.E., and McKee, E.H., 1993, Neogene tectonism from the southwestern Nevada volcanic field to the White Mountains, California; Part 1, Miocene volcanic stratigraphy, paleotopography, extensional faulting and uplift between northern Death Valley and Pahute Mesa, *in* Lahren, M.M., Trexler, J.H., Jr., and Spinosa, C., eds., Crustal evolution of the Great Basin and the Sierra Nevada: Reno, Nevada, University of Nevada, p. 353–369.

Wolf, R.A., Farley, K.A., and Silver, L.T., 1996, Helium diffusion and low temperature thermochronometry of apatite: Geochimica et Cosmochimica Acta, v. 60, p. 4231–4240.

Wolf, R.A., Farley, K.A., and Kass, D.M., 1998, Modeling of the temperature sensitivity of the apatite (U-Th)/He thermochronometer: Chemical Geology, v. 148, p. 105–114.

Zeitler, P.K., Herczeg, A.L., McDougall, I., and Honda, M., 1987, U-Th-He dating of apatite: A potential thermochronometer: Geochimica et Cosmochimica Acta, v. 51, p. 2865–2868.

MANUSCRIPT RECEIVED BY THE SOCIETY 25 APRIL 2002
REVISED MANUSCRIPT RECEIVED 11 DECEMBER 2002
MANUSCRIPT ACCEPTED 17 DECEMBER 2002

Printed in the USA